



Contents lists available at ScienceDirect

Opto-Electronics Review

journal homepage: <http://www.journals.elsevier.com/geo-electronics-review>

Numerical procedures and their practical application in PV modules analyses. Part I: air mass

T. Rodziewicz*, M. Rajfur*

Institute of Biotechnology, University of Opole, ul. kard. B. Kominka 6, 45-032 Opole, Poland

ARTICLE INFO
Article history:

Received 2 November 2018

Received in revised form 3 February 2019

Accepted 8 February 2019

Available online 1 March 2019

Keywords:

Sunlight radiation spectrum

Sunlight radiation intensity

Radiation

Solar power

Solar power industry

ABSTRACT

The subject of the article is aspects of PV modules and cells measurement, with the use of natural sunlight. A light source is an important element during calibration and measurements of solar cells and modules. All designers of artificial light sources try to recreate natural light using so called measurement tables. The correctly performed measurement, i.e. meeting all the appropriate atmospheric conditions, guarantees obtaining the result with the use of a reference spectrum. The article has two main aims. The first aim of the article is to answer the question asked earlier - if the sunlight spectrum registered in appropriate conditions is so good that it serves as the reference spectrum - then, in practice, during measurements carried out with its use, certain problems occur regarding the correct measurement results or their interpretation. The second aim regards presenting detailed numeric procedures in order to enable readers to associate air mass with geographical coordinates and Local Solar Time of their study/laboratory location. Moreover, having the data from their local meteorological station, they will be able to estimate the occurrence of the measurement spectral error of the tested cell/module not only from the group referred to in the article but also for others, for which they have a dedicated characteristics of spectral response.

© 2019 Association of Polish Electrical Engineers (SEP). Published by Elsevier B.V. All rights reserved.

1. Introduction

Measurement of the obtained parameters is a very important part of the design and manufacturing process of solar cells and modules. Two classes of measurements can be emphasised in this area, connected with: precise calibration - to make reference cells/sensors and to document record efficiencies for individual units and routine measurements - to select cells/modules and improve the technological production process. The presented article regards aspects of calibration/measurements with the use of natural sunlight.

The analysis of available works regarding PV cells and modules calibration procedures results in the conclusion that natural sunlight should be a perfect test source. There are, however, many questions, namely: How precisely can a cell/module be measured with the use of sunlight? What are the important atmospheric conditions, which influence the correctness of a measurement? Can measurements be carried out without the use of specialist equipment? How frequently, in practice, does one find the appropriate conditions to carry out the above mentioned measurements?

The precision of calibration with the use of natural sunlight (i.e., correct radiation source spectrum diffusion) is tested with the use of computer modelling of the solar radiation spectrum. For the purpose of this article, the spectrum was generated in the spectrum simulator SMARTS2, for the actual atmospheric/climate conditions, with low air mass optical factor ($AM < 1.5$) and good sky visibility. The presented method requires taking simple and cheap measurements, including only the following elements: Sun's position in the sky (i.e. recording of the time and geographical location of the study site), temperature, humidity and air pressure, global and dispersed (or direct) value of solar radiation intensity. All the important measurement data were generated from the local, automatic weather station owned by the laboratory.

Results of the carried out simulations confirm that the spectrum of the direct component (and total) of solar radiation in the clear sky conditions and low AM value, is a perfect reference for the standard reference spectrum AM 1.5 G - much better than the type obtained from expensive simulators which cost 20 000 USD or more. The PV cells/modules measurements errors obtained with this method of the value 5% are achievable with the use of high-class pyranometers (e.g., CM-11 or CM-21 Kipp & Zonen) to measure radiation intensity, and good quality of other measuring devices of the weather station. The analysis of the climate data for southern Poland shows that the atmospheric conditions required to carry out the above mentioned measurements and calibration are mostly during summer.

* Corresponding authors.

E-mail addresses: trodziewicz@wp.pl (T. Rodziewicz), mrajfur@o2.pl (M. Rajfur).

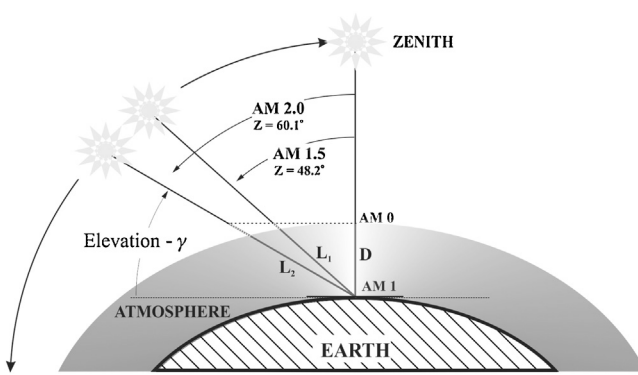


Fig. 1. Graphic presentation of the optical atmosphere mass factor value (AM).

2. Sun position and optical air mass

2.1. Calculation

Air mass optical factor (AM) is the relation of the length of a distance travelled by the optical beam of direct solar radiation through the atmosphere, to its thickness (Fig. 1):

$$AM = \frac{L}{D} \approx \frac{1}{\cos z}. \quad (1)$$

In line with the accepted definition, AM 1 refers to solar radiation in the equator, with the Sun in zenith and the Earth's declination is $\delta = 0^\circ$. In the case of AM 1.5, the angle between the zenith and the radiation direction is 48.2° , and for AM 2 - 60° . The symbol AM 0 refers to solar radiation outside of the Earth's atmosphere.

Approximation of the value of the optical atmosphere mass factor with Eq. (1) is correct only for the angles not larger than 70° (Table 1). If it is necessary to determine AM values for larger angles, one of the below presented formulas should be applied:

a) SANDIA laboratory:

$$AM_p(t) = \frac{p}{p_0} \cdot \left[\cos(z) + 0.50572 \cdot (96.079950^\circ - z)^{-1.6364} \right]^{-1}, \quad (2)$$

where z - n [deg], p - is the local air pressure in bar, p_0 is the reference pressure in bar.

The formula prepared by Kasten and published by: F. Kasten, A. Young [1], and D.L. King, J.A. Kratochvil, and W.E. Boyson [2].

b) Radiation spectrum simulator SMARTS 2 [3,4] – here six different optical air masses are defined, in order to increase the precision of estimating the influence of atmosphere on absorption and diffusion of a solar radiation beam, in particular for the large angles of deviation from the zenith. The first, applied to the basic cases connected with Rayleigh's diffusion – m_R , and others, which describe the phenomena in more detail, i.e. m_a is the diffusing aerosol, m_0 is the ozone occurrence, m_g is the mix of gases, and m_w is the steam:

$$m_i = [\cos(z) + a_{i1} \cdot z^{a_{i2}} \cdot (a_{i3} - z)^{a_{i4}}]^{-1}. \quad (3)$$

For the basic case, i.e. Rayleigh's diffusion, m_i takes m_R , and substituting to (3) for $a_{i1} = 0.45665$, $a_{i2} = 0.07$, $a_{i3} = 96.4836$, $a_{i4} = -1.697$, we obtain:

$$AM_p(t) = \frac{p}{p_0} \cdot \left[\cos(z) + 0.45665 \cdot z^{0.07} \cdot (96.4836^\circ - z)^{-1.697} \right]^{-1}, \quad (4)$$

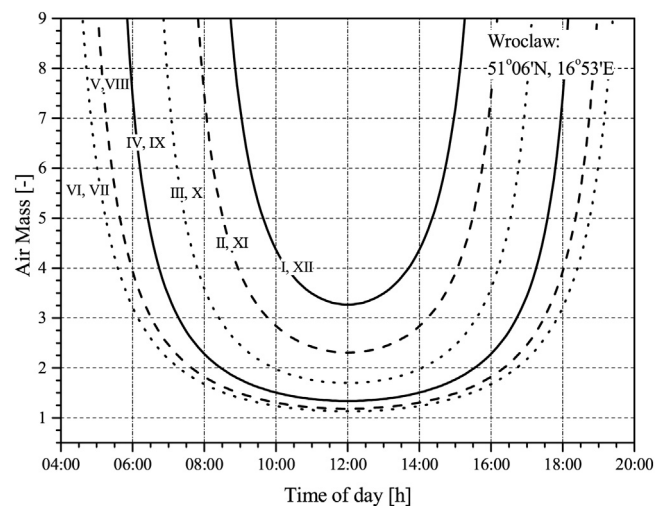


Fig. 2. Values for optical atmosphere AM depending on the time of day (hours) for the 1st day month in year.

where z in [deg].

In the limit case $z = 90^\circ$, optical air mass for Rayleigh's diffusion is of 38.1361 and is very close to the values, e.g. of 38.1665 determined by Miskolczi *et al.* [5] and of 38.0868 by Kasten and Young [1].

c) Radiation spectrum simulator SEDES2 [6]:

$$AM_p(t) = \frac{p}{p_0} \cdot \left[\cos(z) + 0.00094 \cdot (1.6389 - z)^{-1.253} \right]^{-1}, \quad (5)$$

where z in [rad].

d) Radiation spectrum simulator SPECTRAL2 [7]:

$$AM_p(t) = \frac{p}{p_0} \cdot \left[\cos(z) + 0.15 \cdot (93.885^\circ - z)^{-1.253} \right]^{-1}, \quad (6)$$

where z in [deg].

All the above mentioned formulas give very close results (see Table 1). Noticeable differences appear only for the angles much above 85° and do not exceed 0.5% for the angles up to 89° . In the case of the procedure applied in SANDIA Laboratory and used in the simulator SPECTRAL2, their mutual differences do not exceed 1% in the end of their range (i.e., for 90°). Further in the article, all calculations of AM values distribution were made on the basis of the procedure used in SANDIA Laboratory (i.e., based on the relation 2).

Where: z [deg] is the angle of deviation of the component direct beam of solar radiation from the zenith, γ [deg] is the angle of the Sun elevation above the horizon, δ [%] is the percentage value of the difference/error for AM factor determined by the SANDIA Laboratory procedure, used in SMART2 simulator.

Sunbeams incidence angles above 85° are observed in practice during coming in and out of the horizon, when the radiation intensity is very low, at single W/m^2 . Figure 2 presents interrelation of optical atmospheric mass factor (AM) and the time of day for each first day of a month of a year in Wroclaw, Poland ($52^\circ N; 17.1^\circ E$) [8]. The relation (2) and the value of the Sun angular velocity, which is $= 15^\circ/hour$, were used for the calculation. Other necessary relations were taken from Refs. 9–12 and presented below:

$$\alpha_d = 2\pi(d-1)/365, \quad (7)$$

$$E = 3.82 \left[\begin{array}{l} 0.0000075 + 0.001868 \cos(\alpha_d) - 0.032077 \sin(\alpha_d) - 0.014615 \cos(2\alpha_d) \\ - 0.04089 \sin(2\alpha_d) \end{array} \right], \quad (8)$$

Table 1

The numerical value of AM on the sea level.

$z[\text{deg}]$	$\gamma[\text{deg}]$	$1/\cos z$	AM(1)SANDIA	AM(2)SMARTS2	AMSEDES2	AMSPECTRAL2	$\delta [\%] = 100 \cdot AM(1) - AM(2) / AM(1)$
0	90	1.0	1.00	1.00	1.00	1.00	0.029
30	60	1.2	1.15	1.15	1.15	1.15	0.008
60	30	2.0	1.99	1.99	1.99	1.99	0.017
70	20	2.9	2.90	2.90	2.90	2.90	0.025
80	10	5.8	5.58	5.59	5.58	5.58	0.037
85	5	11.5	10.30	10.30	10.33	10.32	0.035
86	4	14.3	12.29	12.30	12.34	12.34	0.036
87	3	19.1	15.13	15.14	15.23	15.22	0.048
88	2	28.7	19.40	19.42	19.56	19.54	0.099
89	1	57.3	26.24	26.32	26.37	26.31	0.288
89.6	0.4	143.2	32.42	32.61	32.17	32.05	0.599
89.7	0.3	191.0	33.65	33.88	33.27	33.13	0.679
89.8	0.2	286.5	34.95	35.22	34.39	34.23	0.772
89.9	0.1	573.0	36.32	36.64	35.55	35.37	0.877
90	0	∞	37.76	38.13	36.71	36.51	0.998

$$t_{sol} = t_{std} + \frac{L_{st} - L}{15} + E, \quad (9)$$

$$\omega = (t_{sol} - 12h) \frac{\pi}{12h}, \quad (10)$$

$$\begin{aligned} \delta &= 0.006918 - 0.399912 \cos \alpha_d + 0.070257 \sin \alpha_d \\ &- 0.006758 \cos 2\alpha_d + 0.000907 \sin 2\alpha_d \\ &- 0.002697 \cos 3\alpha_d + 0.00148 \sin 3\alpha_d, \end{aligned} \quad (11)$$

$$z = \cos^{-1}(\cos \varphi \cos \delta \cos \omega + \sin \varphi \sin \delta), \quad (12)$$

where:

α_d – the angle at which the Earth orbits around the Sun in [rad]; d – the number of the day in a year; ω - the value of the sun location angle on the horizon in [rad] (negative before noon, positive in the afternoon, at noon 0° and increases $15^\circ/\text{hour}$); t_{sol} – solar time (i.e. astronomical); t_{std} – local time (zone) in [h]; L_{st} – geographical longitude for the time zone location in [deg]; L – geographical longitude for the study object location in [deg]; E – standard time expression - i.e. adjustment of duration of astronomical day resulting from the Earth rotation and the Sun movement on elliptic orbit, as the function of the Earth rotation angle around the Sun (α_d) in [h]; z – the angle between the falling beam and the horizon in [deg], δ – value of solar declination, as a function of the Earth rotation around the Sun in [rad]; φ – geographical latitude of a location.

2.2. The influence of AM value on the intensity of solar radiation

The intensity of solar radiation falling on the Earth horizon, its structure (i.e., the content of the diffuse component) and the shape of radiation spectrum depend on: momentary value of solar radiation intensity in upper atmosphere, geographical location and atmosphere thickness, through which light passes, solar radiation incidence angle, area profile and current meteorological conditions. The value of the radiation reaching upper layers of the Earth's atmosphere (i.e. outside of the atmosphere) is variable, due to the Earth's rotation around the Sun on an elliptical orbit. It fluctuates from 1.33 kW/m^2 in July, when the distance of the Earth to the Sun is the longest ($1.522 \cdot 10^8 \text{ km}$) to 1.42 kW/m^2 in January, at the distance of $1.472 \cdot 10^8 \text{ km}$ [12] (Fig. 3).

Its mean value, at the average distance of the Earth from the Sun ($1.495 \cdot 10^8 \text{ km}$) is called the solar constant I_0 and amounts to $1367 \pm 7 \text{ W/m}^2$ (WMO, Commission for Measurements and Observation Methods, 8th session, Mexico City. 1981). Its momentary

value was estimated by Spencer [10] in the following relation:

$$\begin{aligned} G_{d\text{ external}} &= I_0(1.00011 + 0.034221 \cos \alpha_d + 0.00128 \sin \alpha_d \\ &+ 0.000719 \cos 2\alpha_d + 0.000077 \sin 2\alpha_d). \end{aligned} \quad (13)$$

The component direct beam of solar radiation on the Earth's surface ($G_B(t)$ in [W/m^2]), its stream on the horizon plane [$(G_{B,H})$ in $[\text{W/m}^2]$] and its global value [$(G_{0,H})$ in $[\text{W/m}^2]$] depends on the momentary values of the following factors: atmosphere mass value (AM) and suppression of component direct beam (K_b – beam clear sky index) as follows [6,10,11]:

$$G_B(t) = K_b G_{d\text{ external}} \cdot \cos(z) \approx K_b G_{d\text{ external}} / AM. \quad (14)$$

$$G_{B,H}(t) = G_B(t) \cdot [\cos(\varphi) \cos(\delta) \cos(\omega) + \sin(\varphi) \sin(\delta)]. \quad (15)$$

$$G_{0,H}(t) = G_{B,H}(t) + G_{S,H}(t). \quad (16)$$

2.3. The influence of AM on the distribution of power and energy of solar radiation

The course of the function of AM, determined according to (2) for a given region is a mathematical function with the following variables: time, geographical location and atmospheric pressure. The function does not depend on local atmospheric conditions and its shape is close to paraboloid Fig. 4a), which projections on the XZ and XY planes are frequently published by many authors (for example Fig. 2), when describing the tests conditions of the selected PV cells and modules. The actual diffusion of solar radiation power and energy is the function of AM and strictly depends on the local, specific climate conditions in the region. Figure 5 presents the distribution recorded in southern Poland¹ : a) annual, b) monthly - content of solar radiation energy for various ranges of AM value.

2.4. The influence of AM on the distribution of solar radiation spectrum for a cloudless day

In Fig. 6 the structure of a reference spectrum is presented: AM 0 - in upper layers of the atmosphere, AM 1.5 G – total solar radiation on the POA plane inclined at 37° (according to IEC 60904-3

¹ Determining the distribution of solar radiation energy in the defined ranges of AM variability requires implementing one of the procedures for AM determination, i.e. relation (2-6) and [12] as a function of time. Then, registration of instantaneous values of solar radiation power values with a respective value of AM in a function of time, allow to integrate the power of radiation for the selected AM variability ranges and summing them up for a day, month or year period.

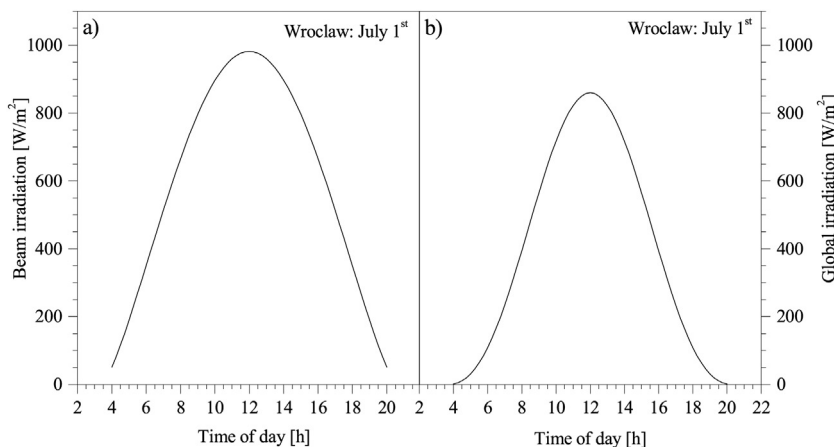


Fig. 3. a) Simulation of the direct component route (in the beam cross-section) - relation (14) and b) total value of solar radiation falling on the horizon plane - relation (16) for Wroclaw, Poland. The estimation assumes 10% of the level of the diffuse component content ($G_{s,h}(t)$ in W/m^2) - a typical value occurring on a July day with cloudless sky.

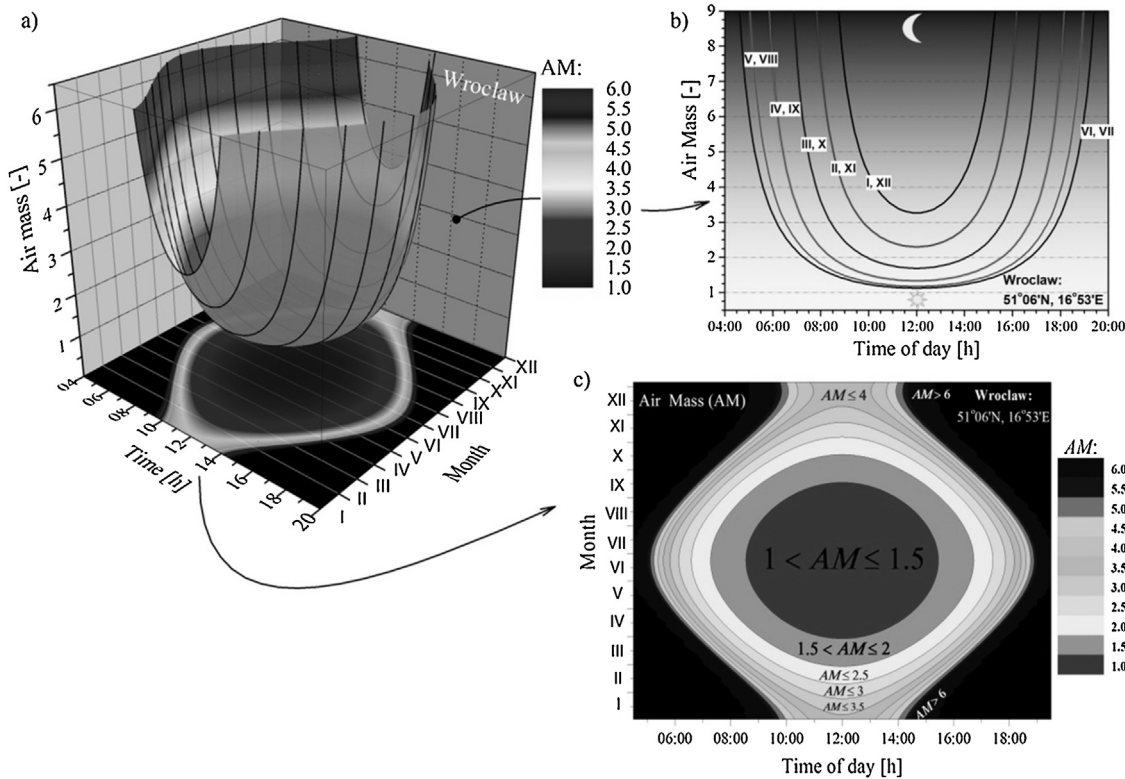


Fig. 4. a) Complete (i.e., 3D) graph of the air mass function and its projections; b) flat graph in the function of the time of day, c) contour graph in the function of the time and day of the year.

[13,14]), AM 1.5D – direct component and diffuse component in the horizon plane (Diffuse_horizon_irradiance). In Figs. 7–8, changes in the distribution of the spectrum of the solar radiation, falling on the horizon plane, for a sunny July day, from 1 to 7 p.m. astronomical time, are presented. The result of simulation with the SMARTS2 program for the atmospheric conditions shown in the figure background which were constant during the analysis, for direct and global component of solar radiation. In Figs. 9–10, changes in the distribution of the spectrum of the solar radiation, falling on the horizon plane, for a sunny July day, in the function of the changes of values of AM. The result of simulation with the SMARTS2 program [4,15,16], for the atmospheric conditions shown in the figure

background,² which were constant during the analysis, for direct and global component of solar radiation respectively. Figures 6–10 were presented for demonstrative purposes. They will get their cognitive value after standardisation of the irradiation intensity values to 1000 W/m^2 (see Fig. 12). The results of standardisation show very little influence of the air mass factor on the changes of solar irradiation spectrum shape, i.e. on the spectral inconsistency error.

² The atmospheric data of a typical, sunny July day in southern Poland, which are input data for the spectrum simulation, are generated automatically by the program, in consequence of the selection in the SMARTS2 program of the following parameters: a reference spectrum as MidLatitude summer, aerosol model as S&F Rural, time and location of the study as well as the data from the local meteorological station.

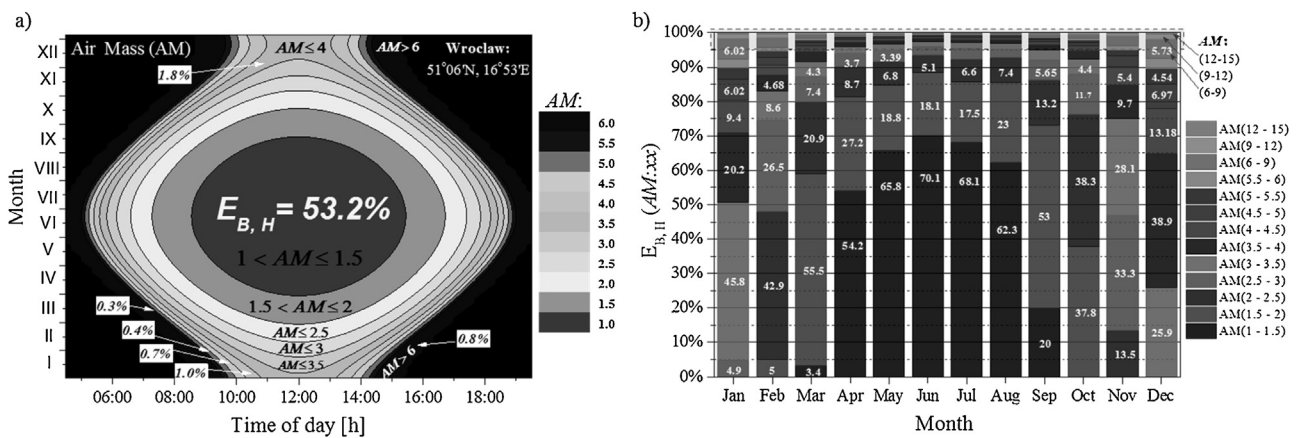


Fig. 5. Solar radiation energy content distribution for various ranges of AM value: a) annual, b) monthly. The studies were carried out for Wrocław, Poland for which AM values distribution was presented in Figs. 4a)-4c).

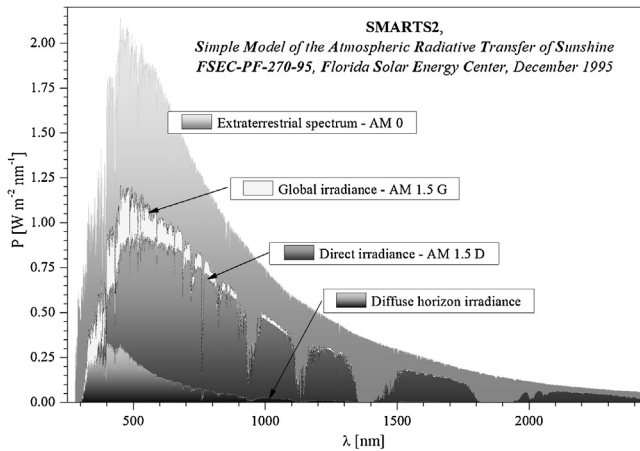


Fig. 6. The structure of a reference spectrum: AM 0 – in upper layers of the atmosphere, AM 1.5 G – total solar radiation on the POA plane inclined at 37° (according to IEC 609043 [13]), AM 1.5D – direct component, and Diffuse.horizon. irradiance – diffuse component in the horizon plane.

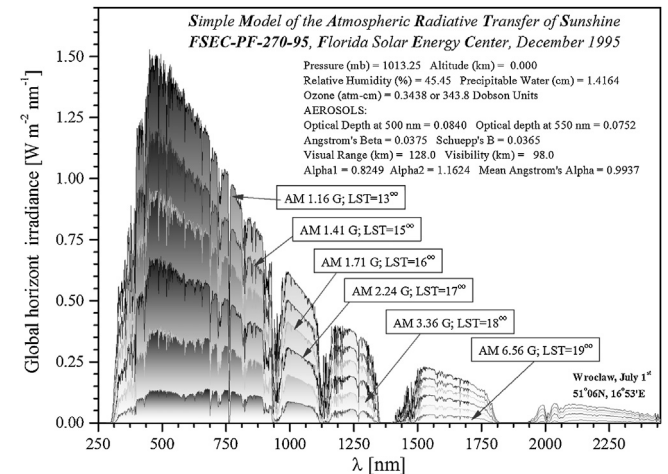


Fig. 8. Changes in the distribution of the total spectrum of the solar radiation, falling on the horizon plane, for a sunny July day, from 1 to 7 p.m. astronomical time (LST). The result of simulation with the SMARTS2 [4] program, for the atmospheric conditions shown in the figure background, which were constant during the analysis.

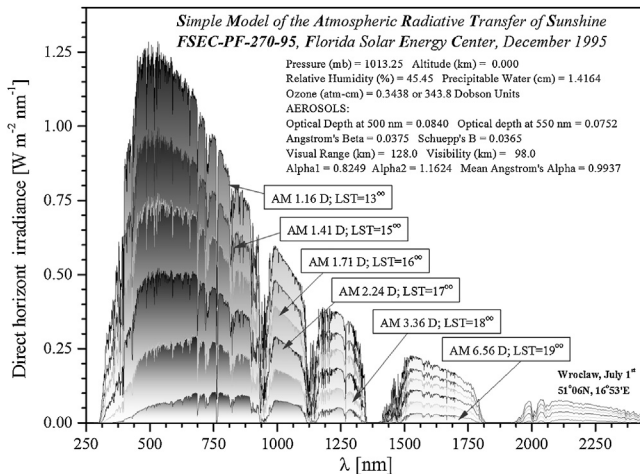


Fig. 7. Changes in the distribution of the spectrum of the solar radiation direct component, falling on the horizon plane, for a sunny July day, from 1 to 7 p.m. astronomical time (LST- Local Solar Time in [h]). The result of simulation with the SMARTS2 [4] program, for the atmospheric conditions shown in the figure background, which were constant during the analysis.

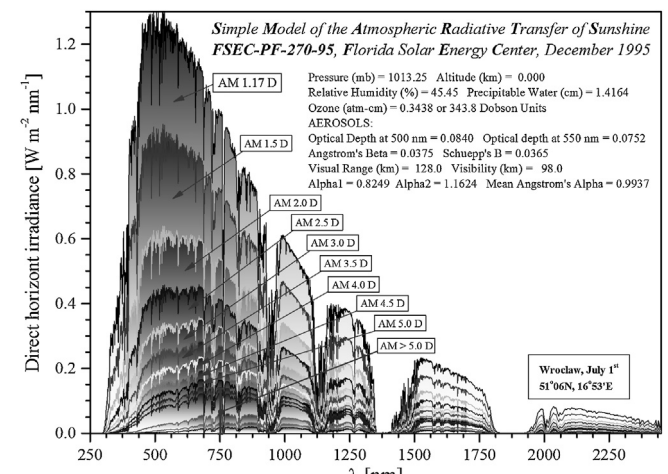


Fig. 9. Changes in the distribution of the spectrum of the solar radiation direct component, falling on the horizon plane, for a sunny July day, in the function of the changes of values of AM. The result of simulation with the SMARTS2 [4] program, for the atmospheric conditions shown in the figure background, which were constant during the analysis.

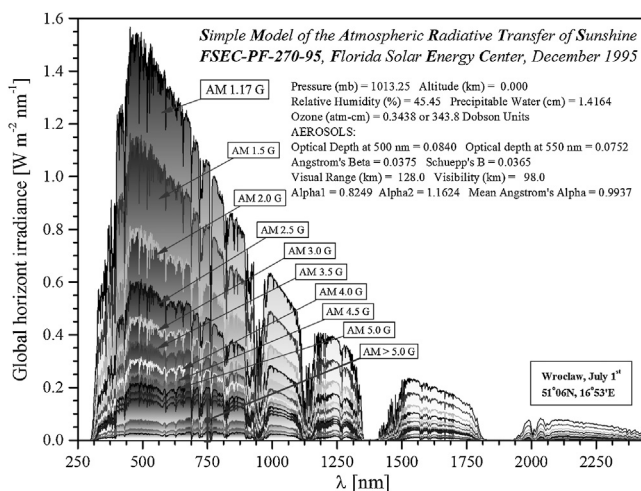


Fig. 10. Changes in the distribution of the total spectrum of the solar radiation direct component, falling on the horizon plane, for a sunny July day, in the function of the changes of values of AM. The result of simulation with the SMARTS2 [4] program, for the atmospheric conditions shown in the figure background, which were constant during the analysis.

3. Practical application of AM for calibration and testing PV cells and modules in field conditions

3.1. Testing in natural sunlight - advantages and disadvantages

Thanks to the precision of solar cells measurement, natural sunlight is, in many aspects, a much better light source than that from solar light simulator (Figs. 11 and 12) [17]. It is perfectly homogeneous for every PV cell or module size, which eliminates errors caused by spatial non-homogeneity of the source. It is very well collimated (regarding direct radiation beam), which makes it easier to remove errors from many reflections. Perfect homogeneity allows to carry out analysis simultaneously in the chamber and reference detector (side-by-side). Also the spectrum of natural light is, in appropriate atmospheric conditions, a perfect reference to standard solar spectrum and, obviously, fits the standard AM 1.5 G much better (Fig. 6) than the spectra of many expensive simulators (Figs. 7–10 and 12). The same conclusion was drawn by (Berman and Faiman, 1997) [18].

The only disadvantage is the fact that the conditions for measurements with the use of natural sunlight make it difficult. The measurements can be carried out only in the appropriate conditions (Fig. 13). However, such limitations are not so difficult to overcome for the manufacturers and designers of solar cells. That is because when all cells are manufactured according to the same procedure and come from the same batch - their spectral responses will be similar. Then, it is necessary to have just one, precisely calibrated cell, which can serve as a reference cell in measurements of the remaining cells/modules, in any solar simulator. Therefore, it is enough to take precise measurements with the use of natural sunlight only from time to time, so the need to wait for the appropriate atmospheric conditions is not so important.

In Fig. 13 the course of standardised current value I_{SC}/G_0 falling on PV modules plane, in the function of AM value - for a sunny spring day was presented [19]. One should note the phenomenon of two coming apart bands of measurement points trajectories,

⁴ Note: only the two distributions were used in analysis for the purpose of this article. One regards 12 o'clock and the other: 9.30 a.m. and 4.30 p.m. on 1 July, as these are extremely different distributions and totally (i.e. with much excess) cover the time of day appropriate for the measurements (see Fig. 2).

as an effect of before noon and after noon spectral inconsistency. For amorphous cells, the difference is even up to: 5% for $AM < 2$; 10% for $AM < 2.5$; and 20% for $AM > 3$. The visible spectral inconsistency/instability (before noon and after noon) causes, for the air mass $AM = 2.7$, uncertainty of the measurement within the ranges: below 1.6% for c-Si and mc-Si; 8.5% for a-Si.SJ and above 11% for a-Si.TJ.

Summing up, natural sunlight is a much better light source to carry out precise measurements of solar cells and modules, than the best sunlight simulators. A single potential problem is spectrum changeability. The following questions can be asked: what influences its change if only the change of air mass does not considerably change the shape of its spectrum? In which atmospheric conditions, the allowed, low spectrum inconsistency error occurs? How often such conditions occur during a year? Is it possible to easily determine that the conditions are appropriate and what range of spectral measurement error can be expected during measurements taking in open space?

3.2. PV cells and modules measurements with the use of solar radiation and the spectral inconsistency error

Testing PV cells and modules with reference to a standard spectrum type AM 1.5 G with the use of natural sunlight can be made in two ways, i.e. using: 1) global solar radiation (i.e. direct component and diffuse component) and 2) only direct component of solar radiation. In both cases, this naturally refers to the radiation falling simultaneously on the whole surface of the measuring equipment.

The first method with the use of global solar radiation seems to be the most appropriate, although not always the most useful [20–23]. In fact, the method is based on the ASTM E1039 standard [24].

In this method, global solar radiation falls from many sides and under various angles, whereas solar light simulator radiation is quite well collimated, which considerably changes measurement conditions. The problem was noticed by several authors, e.g., (Matson, Emery *et al.* 1984) [25]. Another method, in which only a direct component of solar radiation is used, eliminates the above mentioned problem, however, it does not offer the possibility to refer to AM 1.5G spectrum and the actual operating conditions of solar cells and modules. Therefore, the first method was used in further studies, as it better reflects the actual operating conditions of solar cells and modules.

During the measurement, with regard to AM 1.5G, the value of solar radiation direct component intensity is used to "simulate" the global spectrum. It is frequently defined as the difference between the global and diffused value of solar radiation. Estimation of the spectrum requires taking a few simple measurements, in order to measure important atmospheric conditions and estimate spectral inconsistency error. The measurements include: direct and diffused radiation intensity, humidity, air temperature and the Sun location in the sky (i.e. recording of the time and geographical coordinates of the measurement location). The measurements enable to estimate the main factors which influence spectral inconsistency, i.e. air mass, content of saturated water vapour in the air, atmosphere turbidity value [26].

3.2.1. Atmosphere turbidity determination formulas - β , prepared by Guyermann C. A. (1998) [16]

The clean dry atmosphere optical depth is parameterized with [27–30]:

$$\delta_c = f_1(p, m_R)[f_2(u_o, m_R) + f_3(m_R)] + f_4(u_o, m_R) + f_5(u_n, m_R), \quad (17)$$

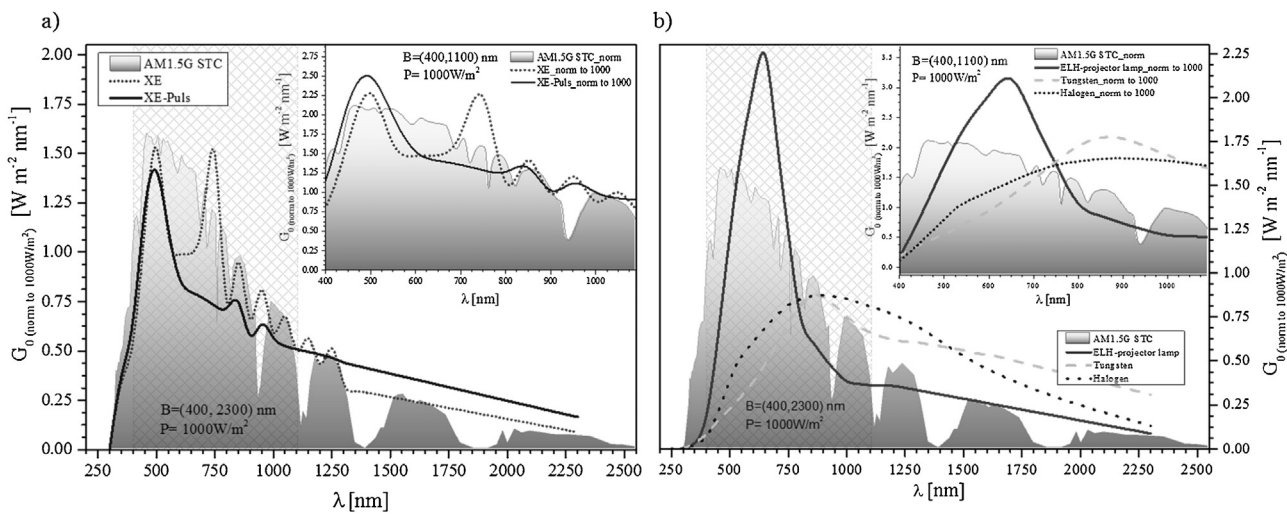


Fig. 11. A comparison of spectral characteristics of the lamps: a) Xenon, b) filament, with AM1.5 G standard [17].

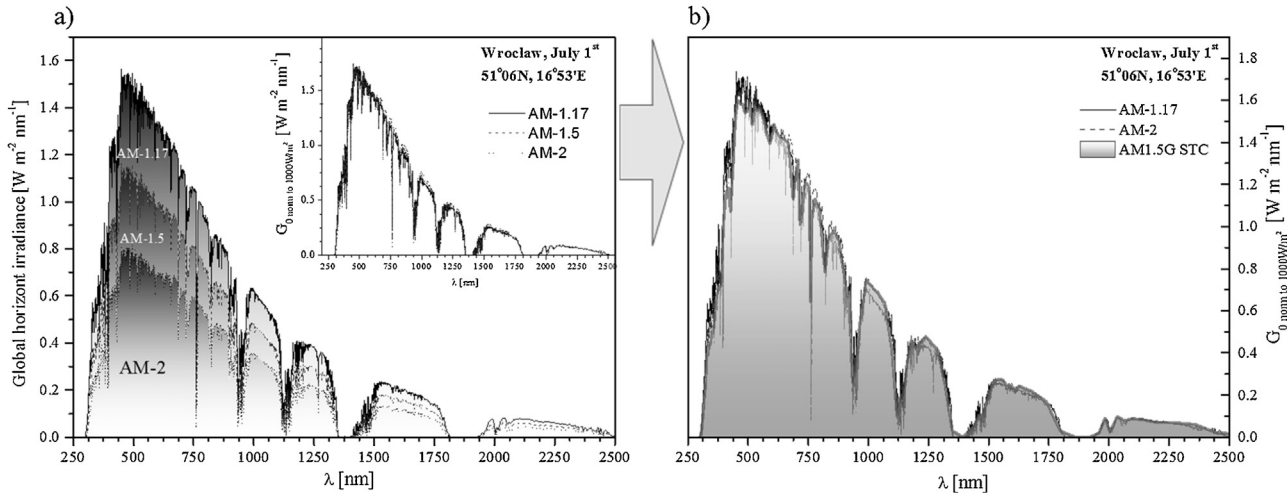


Fig. 12. a) Spectral characteristics of global¹⁴ radiation for AM values: 1.17, 1.5 and 2 falling on the horizon plane. The window in the figure presents a) distributions to the power of 1000 W/m^2 , b) comparison of distribution of spectral characteristics of the global radiation of the value AM 1.17 and 2 with the AM 1.5 G standard.

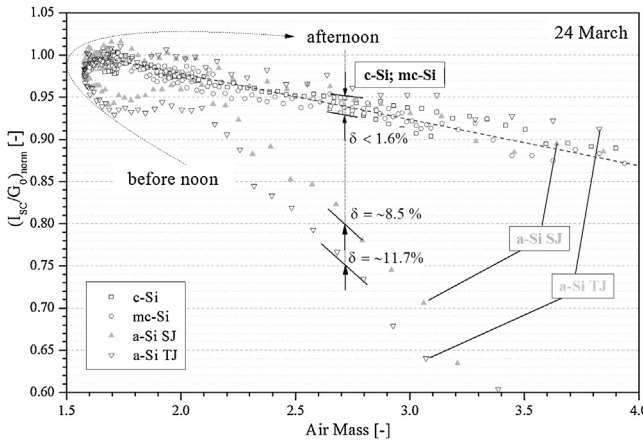


Fig. 13. The influence of solar radiation spectrum inconsistency on the range of uncertainty of cells and modules measurements in open space conditions [19].

where f_1, f_2, f_3, f_4 and f_5 are simple functions whose coefficients are obtained by fitting the numerical data with a least squares' technique, and u_o and u_n are the total amounts of O_3 and NO_2 in a vertical column, respectively.

Defining:

$$q = 1 - p/p_0, \quad (18)$$

where $p_0 = 1013.25 \text{ mb}$, the following parameterizations are proposed.

$$f_1 = (a_0 + a_1 m_R) / (1 + a_2 m_R), \quad (19)$$

$$f_2 = b_0 + b_1 m_R^{0.25} + b_2 \ln(m_R), \quad (20)$$

$$f_3 = \frac{(0.19758 + 0.00088585 m_R - 0.097557 m_R^{0.25})}{1 + 0.0044767 m_R}, \quad (21)$$

$$f_4 = (c_0 + c_1 m_R^{-0.72}) / (\exp(1 + c_2 m_R)), \quad (22)$$

$$f_5 = u_n [2.8669 - 0.078633 \ln^{2.36}(m_R)], \quad (23)$$

$$a_0 = 1 - 0.98173 q, \quad (24)$$

$$a_1 = 0.18164 - 0.24259 q + 0.050739 q^2, \quad (25)$$

$$a_2 = 0.18164 - 0.17005 q - 0.0084949 q^2, \quad (26)$$

$$b_0 = -0.0080617 + 0.028303 u_o - 0.014055 u_o^2, \quad (27)$$

$$b_1 = 0.011318 - 0.041018 u_o + 0.023471 u_o^2, \quad (28)$$

$$b_2 = -0.0044577 + 0.016728u_o - 0.01091u_o^2, \quad (29)$$

$$c_0 = 0.0036916 + 0.047361u_o + 0.0058324u_o^2, \quad (30)$$

$$c_1 = 0.015471 + 0.061662u_o - 0.044022u_o^2, \quad (31)$$

$$c_2 = 0, 039904 - 0, 038633u_o + 0, 054899u_o^2. \quad (32)$$

Similarly, the broadband water vapor optical depth is obtained from:

$$\delta_w = M[g_1 + g_2Mm_w + g_3(Mm_w)^{1.28}]/(1 + g_4Mm_w), \quad (33)$$

where m_w is calculated from:

$$m_w = [\cos(z + 0.031141 \cdot z^{0.1} \cdot (96.4710 - z)^{-1.3814})]^{-1}. \quad (34)$$

However, the air mass functions: m_w, m_R, m_n, m_a in the range of $z < 70^\circ$ angles obtain almost identical values. Noticeable differences between them occur for the angles larger than 80° . Other formulas are presented below:

$$M = \frac{1.7135 + 0.10004m_w + 0.00053986m_w^2}{1.7149 + 0.097294m_w + 0.002567m_w^2}, \quad (35)$$

$$g_1 = (\gamma_1 w + \gamma_2 w^{1.6})/(1 + \gamma_3 w), \quad (36)$$

$$g_2 = (\phi_1 w + \phi_2 w^{1.6})/(1 + \phi_3 w), \quad (37)$$

$$g_3 = (\kappa_1 w + \kappa_2 w^{1.6})/(1 + \kappa_3 w), \quad (38)$$

$$g_4 = (\nu_1 w + \nu_2 w^{0.62})/(1 + \nu_3 w + \nu_4 w^2), \quad (39)$$

$$\gamma_1 = (1.728 - 2.1451q)/(1 - 0.96212q), \quad (40)$$

$$\gamma_2 = (0.3145 + 0.64537q)/(1 - 0.94528q), \quad (41)$$

$$\gamma_3 = (3.5145 - 0.12483q)/(1 - 0.34018q), \quad (42)$$

$$\phi_1 = (0.63889 - 0.81121q)/(1 - 0.79988q), \quad (43)$$

$$\phi_2 = (0.06836 - 0.49008q)/(1 + 4.7234q), \quad (44)$$

$$\phi_3 = (2.1567 + 1, 4546q)/(1 + 0, 038808q), \quad (45)$$

$$\kappa_1 = (-0.1857 + 0.23871q)/(1 - 0.84111q), \quad (46)$$

$$\kappa_2 = (-0.022344 - 0.19312q)/(1 + 6.2169q), \quad (47)$$

$$\kappa_3 = (2.1709 + 1.6423q)/(1 + 0.062545q), \quad (48)$$

$$\nu_1 = 3.3704 + 6.809q, \quad (49)$$

$$\nu_2 = (12.487 - 18.517q - 0.4089q^2)/(1 - 1.4104q), \quad (50)$$

$$\nu_3 = (2.5024 - 0.56834q - 1.4623q^2)/(1 - 1.0252q), \quad (51)$$

$$\nu_4 = (-0.030833 - 1.172q - 0.98878q^2)/(1 + 31.546q), \quad (52)$$

Where, w is the saturated water content in atmosphere is determined according to Eq. (68). Finally, the broadband aerosol optical depth is obtained as:

$$\delta_a = \beta(s_1 + s_2\beta), \quad (53)$$

$$\delta_a = (1/m_a) [\ln(G_{dexteren}/G_B) - m_R\delta_c - m_w\delta_w - m_n\delta_n], \quad (54)$$

$$w = 0.1 \left(0.4976 + 1.5265 \frac{T_{amb}}{273.15} + \exp \left[13.6897 \frac{T_{amb}}{273.15} - 14.9188 \left(\frac{T_{amb}}{273.15} \right)^3 \right] \right), \quad (68)$$

$$\left(216.7 \frac{RH}{100T_{amb}} \exp \left[22.33 - 49.14 \frac{100}{T_{amb}} - 10,922 \left(\frac{100}{T_{amb}} \right)^2 - 0.39015 \frac{T_{amb}}{100} \right] \right).$$

$$\delta_n = u_n [2.8669 - 0.078633 \cdot (\ln(m_n))^{2.36}] . \quad (55)$$

Where, for $\alpha = 1.3$ (α -Angstrom wavelength exponent for the whole spectrum).

$$s_1 = (d_0 + d_1 m_a)/(1 + d_2 m_a), \quad (56)$$

$$s_2 = (h_0 + h_1 m_a + h_2 m_a^2) / (1 + h_3 m_a^n), \quad (57)$$

$$d_0 = (1.6685 + 4.1257w + 0.018748w^2) / (1 + 2.33w), \quad (58)$$

$$d_1 = (0.075379 + 0.066532w - 0.0042634w^2) / (1 + 1.9477w), \quad (59)$$

$$d_2 = (0.12867 + 0.24264w + 0.0087874w^2) / (1 + 3.3566w), \quad (60)$$

$$h_0 = (-0.032335 - 0.0060424w) / (1 + 0.023563w), \quad (61)$$

$$h_1 = (-0.38229 - 0.0009926w) / (1 + 0.044137w^{0.594}), \quad (62)$$

$$h_2 = (-0.0059467 + 0.0054054w) / (1 + 0.91487w), \quad (63)$$

$$h_3 = (0.21989 + 0.041897w) / (1 + 0.35717w), \quad (64)$$

and

$$n = (1.3211 + 2.2036w) / (1 + 1.9367w). \quad (65)$$

Considering that for $z < 70^\circ$, $m = m_R = m_a = m_n = m_w$ then from solving Eq. (53) we obtain the final formula for atmosphere turbidity:

$$\beta = \frac{s_1}{2s_2} \left(-1 + \sqrt{1 + 4 \frac{s_2 \delta_a}{s_1^2}} \right). \quad (66)$$

The following Table 2 presents test vectors for verification of correctness of implementation of the β atmosphere turbidity calculations algorithm, in the case of its implementation in a reader's own numeric procedures.

The nomographs for determining the atmosphere turbidity value in the function of AM and so called reduced value of intensity component direct beam of solar radiation (G_{Bred} in [W/m^2]), at variable content of steam in atmosphere, are presented in Fig. 14. The idea of the reduced value of intensity component direct beam of solar radiation, G_{Bred} according to Eq. (67):

$$G_{Bred} = G_B \cdot \frac{1367}{G_{dextern}}, \quad (67)$$

where: $G_{dextern}$ is the daily value of solar radiation intensity in the upper layers of atmosphere in [W/m^2], according to (13), $G_B = (G_{0,H} - G_{S,H})/\cos(z)$ – see (12) and (15–16),

- introduced to simplify the nomograph and not define it for individual months in a year.

The turbidity nomographs (Fig. 14) were determined in line with the procedures demonstrated by Gueymard. C. A. (1998) and included in ref. 16 for the following atmospheric conditions: $P_{atm} = 1013$ mbar, total content: ozone $u_o = 0.34$ atm-cm and NO_2 $u_n = 0.2$ matm-cm ($2 \cdot 10^{-4}$ atm-cm). According to Keogh W. and Blakers A.W [26], the declared accuracy of the determined nomographs (Fig. 14) of atmosphere turbidity is ± 0.02 for the conditions:

$P_{atm} = 800 \div 1020$ mbar, $u_o = 0.24 \div 0.44$ atm-cm, $u_n = 0.1 \div 5$ matm-cm.

3.2.2. Distribution of water vapour

Equations (68) prepared by Gueymard C. A. and others [26,31,32] were used to calculate saturated vapour value:

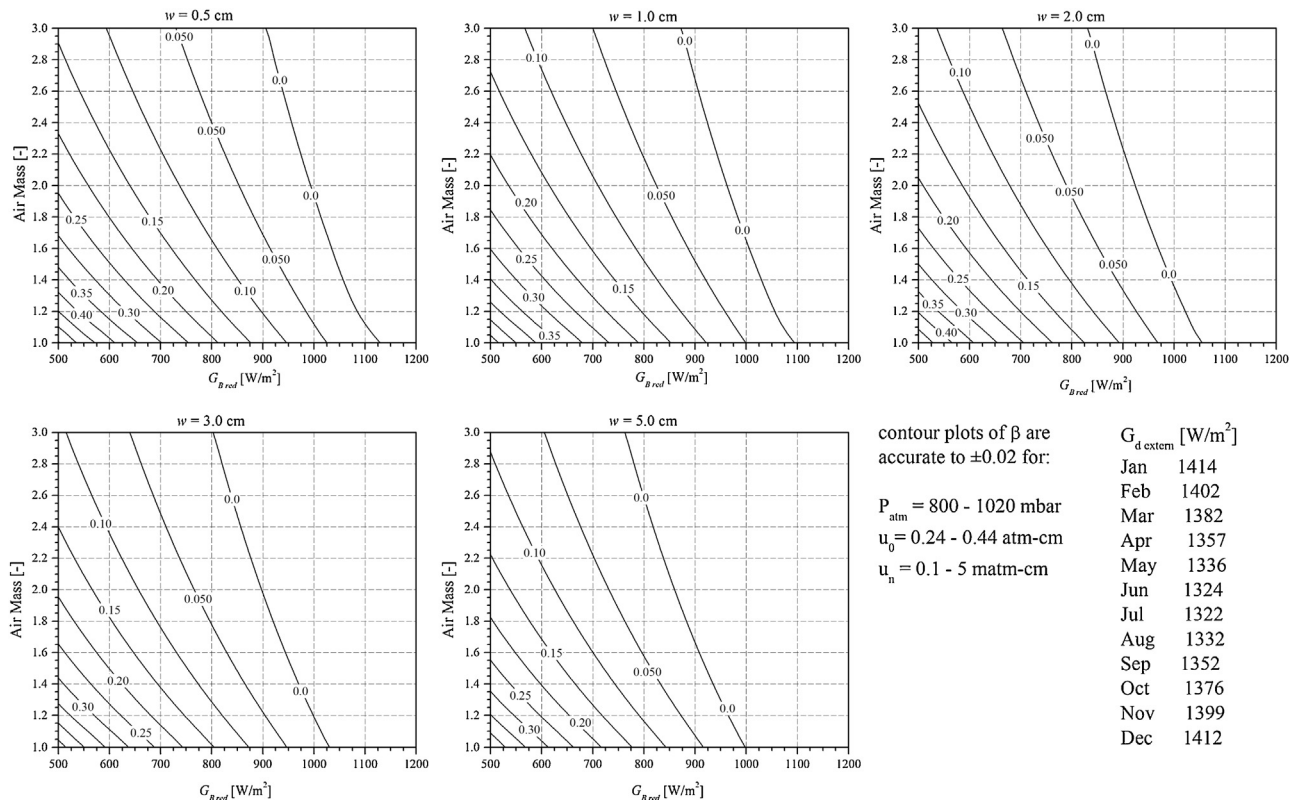
$$w = 0.1 \left(0.4976 + 1.5265 \frac{T_{amb}}{273.15} + \exp \left[13.6897 \frac{T_{amb}}{273.15} - 14.9188 \left(\frac{T_{amb}}{273.15} \right)^3 \right] \right), \quad (68)$$

where:

Table 2

Test vectors for verification of correctness of implementation of the atmosphere turbidity calculations (beta) - β .

Lp	P_{atm}	u_0	m	u_n	w	G_B	q	G_{Bext}	δ_c	δ_w	δ_n	δ_a	β
1	1013	0.34	1	2.00E-04	1	900	0.0002467	1367	0.1195	0.1119	0.0006	0.1860	0.1154
2	1013	0.34	1.2	2.00E-04	1	900	0.0002467	1367	0.1145	0.1004	0.0006	0.1329	0.0829
3	1013	0.34	1.5	2.00E-04	1	900	0.0002467	1367	0.1084	0.0879	0.0006	0.0817	0.0515
4	950	0.2	2	1.00E-02	3	500	0.0624228	1300	0.0933	0.1071	0.0283	0.2490	0.1629
5	950	0.2	2.5	1.00E-02	3	500	0.0624228	1300	0.0879	0.0943	0.0280	0.1720	0.1137
6	950	0.2	3	1.00E-02	3	500	0.0624228	1300	0.0834	0.0851	0.0277	0.1223	0.0818



contour plots of β are accurate to ± 0.02 for:
 G_{dextem} [W/m²]
Jan 1414
Feb 1402
Mar 1382
Apr 1357
May 1336
Jun 1324
Jul 1322
Aug 1332
Sep 1352
Oct 1376
Nov 1399
Dec 1412

Fig. 14. The β atmosphere turbidity nomograph in the function of AM value, reduced value of solar radiation direct component intensity value and water content in atmosphere. The graphic setup from Ref. 26 was the basis for the nomograph. The mean values of G_{dextem} for each month of the year are presented next to the legend.

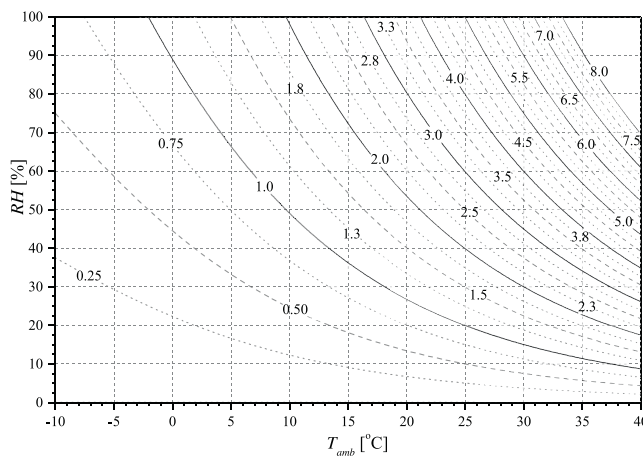


Fig. 15. Nomograph of vapour content in atmosphere (w) in the function of humidity (RH) and ambient temperature (T_{amb}).

w is the estimated thickness of condensed vapour layer in [cm], T_{amb} is the ambient temperature in [K], RH is the relative air humidity in [%]. The obtained data is presented in Fig. 15.

Figure 15 was prepared in the form of a nomograph for fast determination of vapour content for analyses. To determine the accuracy of this method (Gueymard C. A. 1993) [31] compared the predictions of Eq. (68) to accurate measurements from various sources at Sault Ste. Marie, on the USA/Canada border. Monthly average values of surface temperature, surface humidity, and radiosonde soundings were used. He found that the predictions of Eq. (68) were within the $\pm 10\%$ scatter of the accurate measurements. For an instantaneous measurement, the prediction may be a little less accurate than for the monthly averages. As a conservative limit, (Gueymard 1998) [16] uses an accuracy of $\pm 20\%$ for the surface humidity method. When " w " < 0.5 cm, this method becomes less accurate [16].

In Fig. 16 the actual distribution of vapour in atmosphere is presented, as observed during the period of research in Wrocław. Precipitable water " w " is the total amount of water in a vertical column of the atmosphere. It is usually specified in terms of centimetres of liquid water. Water causes heavy absorption in bands in the IR beyond 900 nm. In temperate locations, " w " is usually in the range of 1–3.7 cm. In tropical locations " w " may be as high as 5 cm. In deserts or below freezing conditions, " w " may be as low as 0.5 cm.

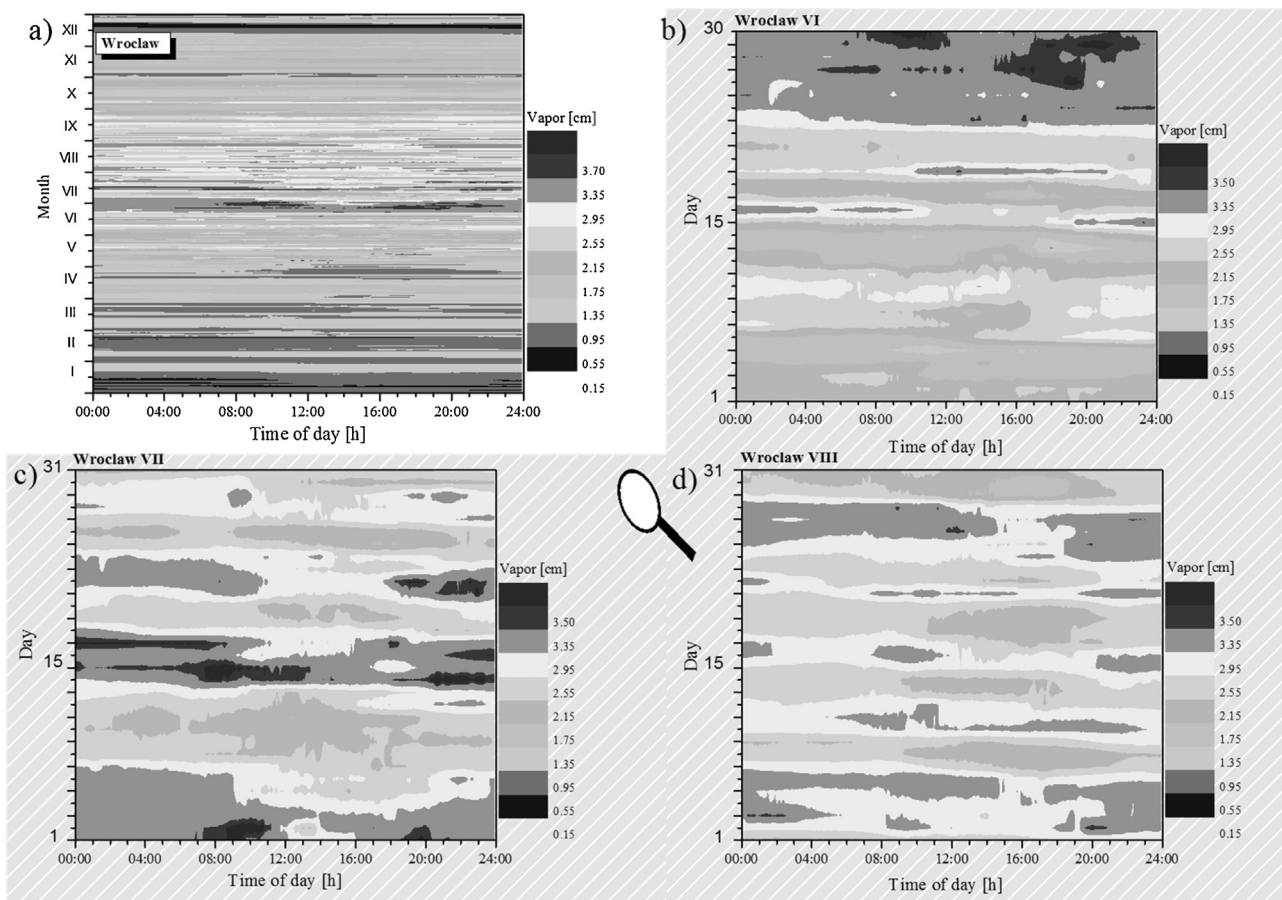


Fig. 16. The value of saturated vapour in atmosphere ($[w]$ = cm) for southern Poland during the period of research. In the enlarged field (blue) - its momentary values from three summer months.

3.2.3. The influence of the light spectral inconsistency on uncertainty of PV modules measurements

The reference spectrum recommended by IEC904-3 [13,14] for measuring and calibration of PV cells and modules is the global solar radiation spectrum (direct + diffuse) with air mass $AM=1.5$, falling on the exposition plane facing south and inclined at 37° vs. the horizon, for the following atmospheric conditions:

- a cloudless day;
- atmospheric water content: 1.4164 cm;
- atmosphere ozone content: 0.3438 atm-cm;
- turbidity: 0.084 at 500 nm which corresponds to beta factor (β) = 0.0316.

As demonstrated in Fig. 13, in natural conditions, even for the same day, spectral distribution of solar radiation of the same AM from before and after noon is different, which results in different measurement outputs for the same PV cells and modules. The measurements taken then carry so called solar light spectral inconsistency error. The error value varies from cell and module (see Fig. 13.) and directly depends on their spectral characteristics (SR) [33,34].

In order to make sure that solar light radiation spectrum used in the study is appropriate for the reference one and to estimate the value of spectral inconsistency error value in the light used for measurements, for typical cells and modules with characteristics

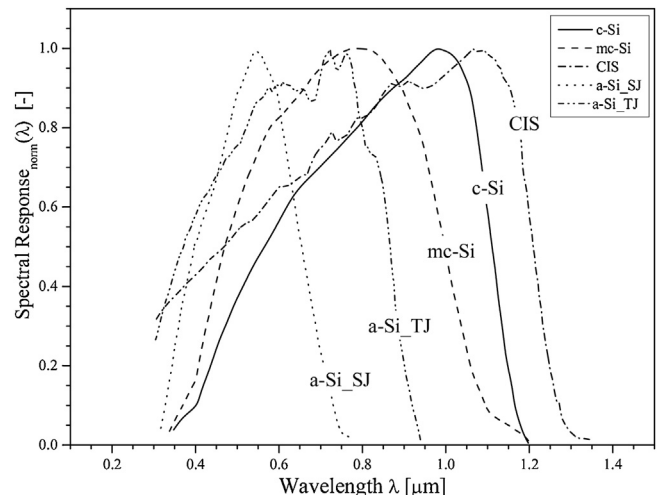


Fig. 17. Characteristics of spectral response of typical, commercial PV modules, referred to in further analyses – where the individual symbols mean: c-Si are the crystalline modules, mc-Si is the polycrystalline, CIS are the modules from CIS, a-Si_SJ are the modules from amorphous silicon one and a-Si_TJ – and three-junction.

from Fig. 17, a spectral inconsistency error function was introduced (ε_M), determined in the following way:

$$\varepsilon_M = \left| 1 - M \right| \cdot 100\% = \left| 1 - \frac{J_{SC}(AM; \beta; w)_{norm_1000W/m^2}}{J_{STC}(\text{Ref. IEC 60904-3})} \right|. \quad (69)$$

Whereas:

$$J_{SC}(AM; \beta; w) = \int_{\lambda_1}^{\lambda_2} SR_{PV}(\lambda) \cdot E(AM; \beta; w; \lambda) d\lambda \quad (70)$$

and its value with adjustment of the radiation value to 1000 W/m² (71):

$$\begin{aligned} J_{SC}(AM; \beta; w)_{norm_1000W/m^2} &= \\ &= \int_{\lambda_1}^{\lambda_2} SR_{PV}(\lambda) \cdot E(AM; \beta; w; \lambda) d\lambda \cdot \frac{1000[W/m^2]}{\int_{0.3\mu m}^{2.8\mu m} SR_{Ref.Det}(\lambda) \cdot E(AM; \beta; w; \lambda) d\lambda} \end{aligned} \quad (71)$$

$$J_{STC}(\text{Ref. IEC 60904-3}) =$$

$$\int_{\lambda_1}^{\lambda_2} SR_{PV}(\lambda) \cdot E_{Ref.IEC 60904-3}(\lambda) d\lambda \cdot \frac{1000[W/m^2]}{\int_{0.3\mu m}^{2.8\mu m} SR_{Ref.Det}(\lambda) \cdot E_{Ref.IEC 60904-3}(\lambda) d\lambda} \quad (72)$$

Then, the spectral adjustment factor (M) takes the form (73):

$$\begin{aligned} M &= \frac{J_{SC}(AM; \beta; w)_{norm_1000W/m^2}}{J_{STC}(\text{Ref. IEC 60904-3})_{norm_1000W/m^2}} \\ &= \frac{\int_{\lambda_1}^{\lambda_2} SR_{PV}(\lambda) \cdot E(AM; \beta; w; \lambda) d\lambda}{\int_{\lambda_1}^{\lambda_2} SR_{PV}(\lambda) \cdot E_{Ref.IEC 60904-3}(\lambda) d\lambda} \cdot \\ &\quad \frac{\int_{0.3\mu m}^{2.8\mu m} SR_{Ref.Det}(\lambda) \cdot E_{Ref.IEC 60904-3}(\lambda) d\lambda}{\int_{0.3\mu m}^{2.8\mu m} SR_{Ref.Det}(\lambda) \cdot E(AM; \beta; w; \lambda) d\lambda} \end{aligned} \quad (73)$$

$$SR_{Ref.Det}(\lambda) = \begin{cases} k; & \lambda \in (0.3; 2.8)\mu m \\ 0 & \lambda \notin (0.3; 2.8)\mu m \end{cases}, \quad (74)$$

where: $SR_{PV}(\lambda)$ is the spectral response of the measured PV cell/module; $SR_{Ref.Det}(\lambda)$ is the accepted model of the pyranometer spectral resolution characteristics; $B_{Ref.Det} = (0.3; 2.8)\mu m$ is the bandwidth of a typical pyranometer (e.g. K&Z CM21) [35,36]; $E_{Ref.IEC 60904-3}(\lambda)$ is the reference spectrum, according to IEC904-3; $E(AM; \beta; w; \lambda)$ is the spectrum of the actual solar radiation for

the defined conditions; $\int_{0.3\mu m}^{2.8\mu m} SR_{Ref.Det}(\lambda) \cdot E_{Ref.IEC 60904-3}(\lambda) d\lambda$ and

$\int_{0.3\mu m}^{2.8\mu m} SR_{Ref.Det}(\lambda) \cdot E(AM; \beta; w; \lambda) d\lambda$ are the value of power of the

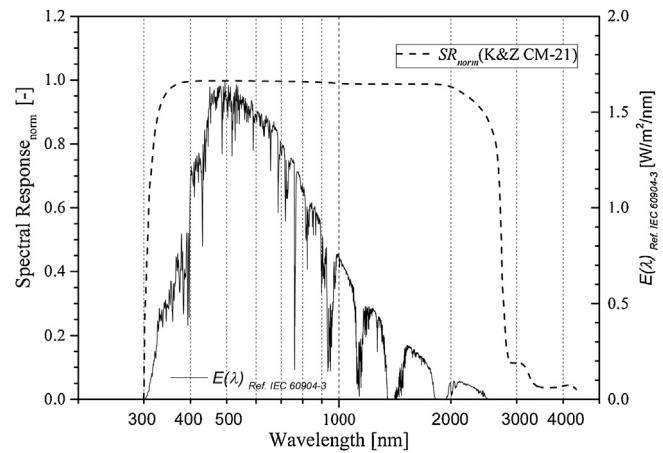


Fig. 18. Spectral response of the pyranometer K&Z CM-21 [35,36] and the reference spectrum distribution recommended by IEC 60 904-3.

reference and actual radiation, shown by pyranometer with bandwidth $B_{Ref.Det}$ and spectral response characteristics $SR_{Ref.Det}(\lambda)$; λ_1 and λ_2 are the lower and upper range of “characteristics cut-off” in spectral response of the measured PV module.

For the reference spectrum recommended by IEC904-3 and the conforming spectra and most frequently occurring atmospheric conditions in the south of Poland and areas in higher latitudes - the values of current densities for individual cells and modules were calculated, according to Eqs. (71) and (72). The natural sunlight spectra were simulated with the spectrum model SMARTS2³ [37], according to Table 3 - i.e., input conditions and parameters. These distributions were additionally standardized to 1000 W/m² in a bandwidth $B_{Ref.Det} = (300; 2800)$ nm – in order to adjust to the operating range of a typical pyranometer (e.g., K&Z CM-21 – see Fig. 18).

The determined spectral inconsistency error function [Eq. (69)] was drawn for each cell/module, with Spectral Response characteristics from Fig. (17), in the form of contour graphs (see - Figs. 19–23), where in the drawing for AM 1.5 the location of a reference spectrum, recommended by IEC904-3, was additionally marked. Placing the location of a reference spectrum allows to observe the sensitivity of spectral inconsistency error function of a cell/module to changes of atmospheric parameters.

Even a quick analysis of the obtained results allows to draw the following conclusions (see Figs. 19–23):

- 1 The consequences of atmosphere turbidity and precipitable water on the value of the spectral inconsistency error of solar light mutually compensate. In the case of high water content in the air, it is better if it is turbid at the same time. This is the case in actual conditions. Nature performs the adjustment. Both turbidity and precipitation of water are higher in the summer and in locations closer to the equator.
- 2 It is important to notice that in adverse atmospheric conditions (i.e., high AM value, high turbidity, low content of steam in atmosphere), spectral inconsistency will have the tendency to, for example, overstate I_{SC} for polycrystalline cells and underestimate for amorphous cells. This is an adverse tendency. In those difficult conditions, the spectrum is too red (high turbidity of air

³ SMARTS2 (Simple Model of the Atmospheric Radiative Transfer of Sunshine) – algorithm of the sunshine radiation spectrum synthesis for a cloudless day, by C. Gueymard, described in Ref. 37. The value of the spectrum synthesis error declared by the author for the set atmospheric conditions, is 5% within the range of (420 and 1100) nm, i.e. within the operation range of the spectroradiometer LiCOR LI-1800 which was used for validation.

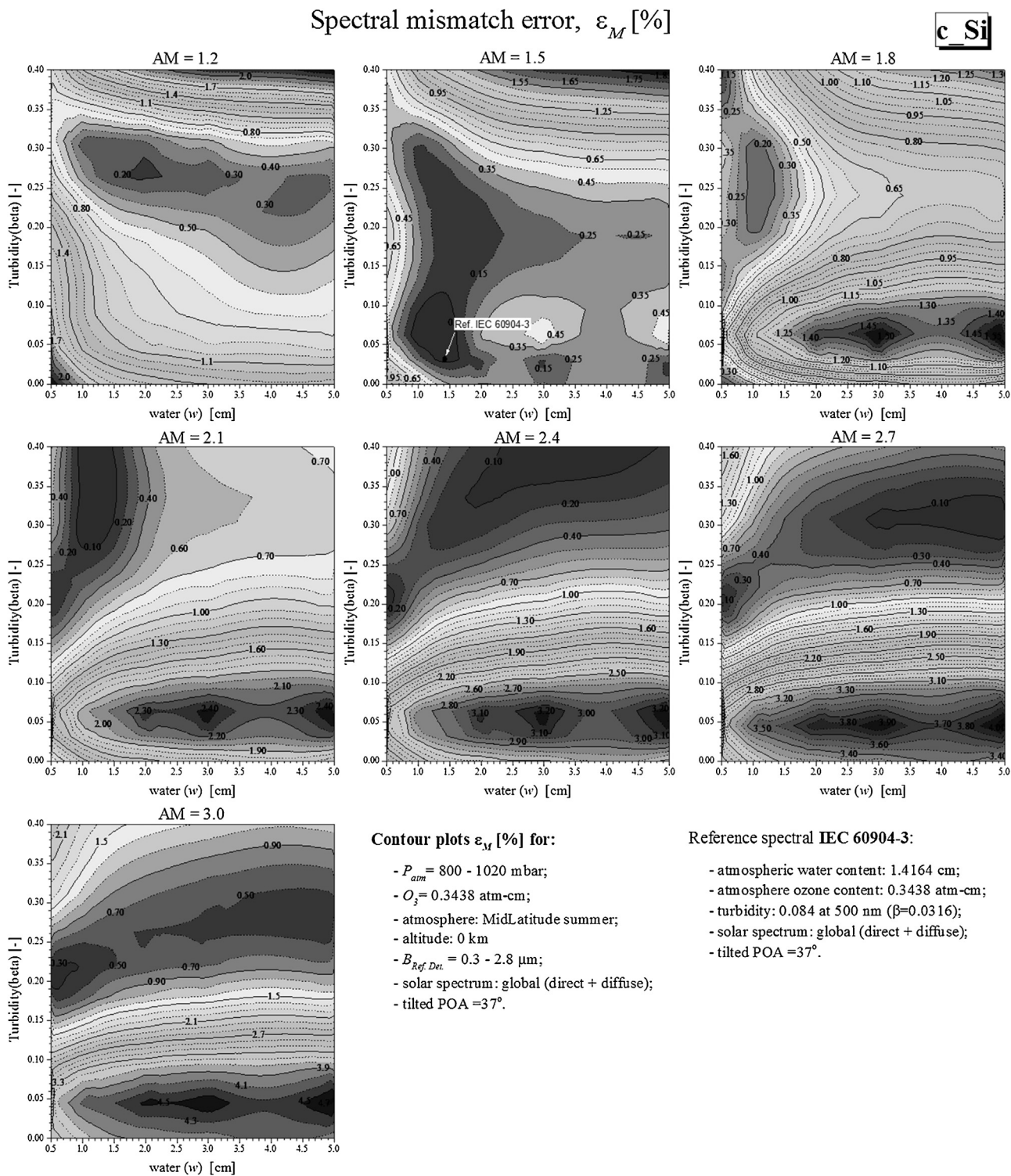


Fig. 19. Graphs of the spectral inconsistency error function (ε_M) for measurements of crystalline (c-Si) cells/modules, in open space conditions on a cloudless day. The results refer to the summer period in Central Europe and the conditions presented in the background of the figure.

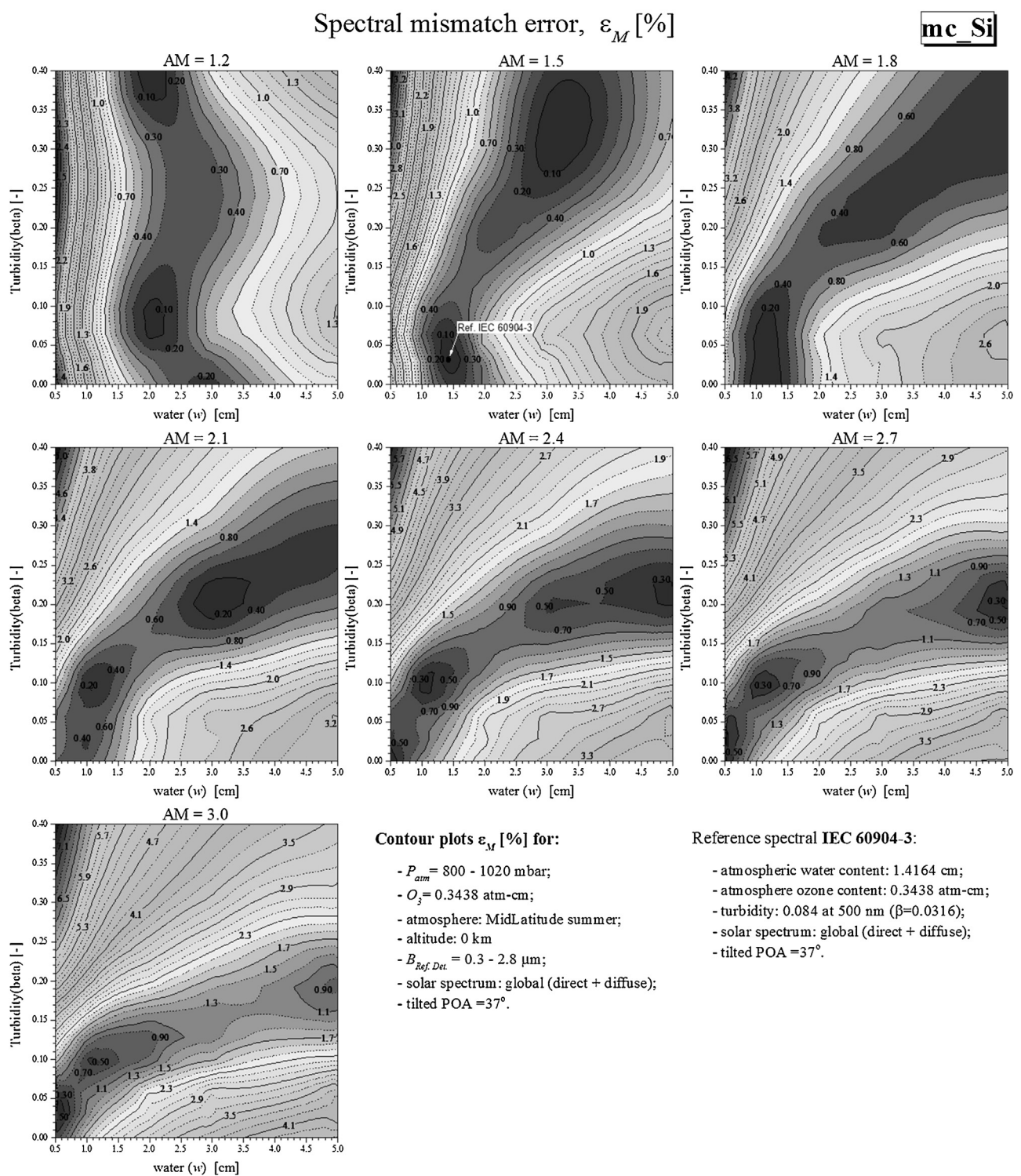


Fig. 20. Graphs of the spectral inconsistency error function (ε_M) for measurements of polycrystalline (mc-Si) cells/modules, in open space conditions on a cloudless day. The results refer to the summer period in Central Europe and the conditions presented in the background of the figure.

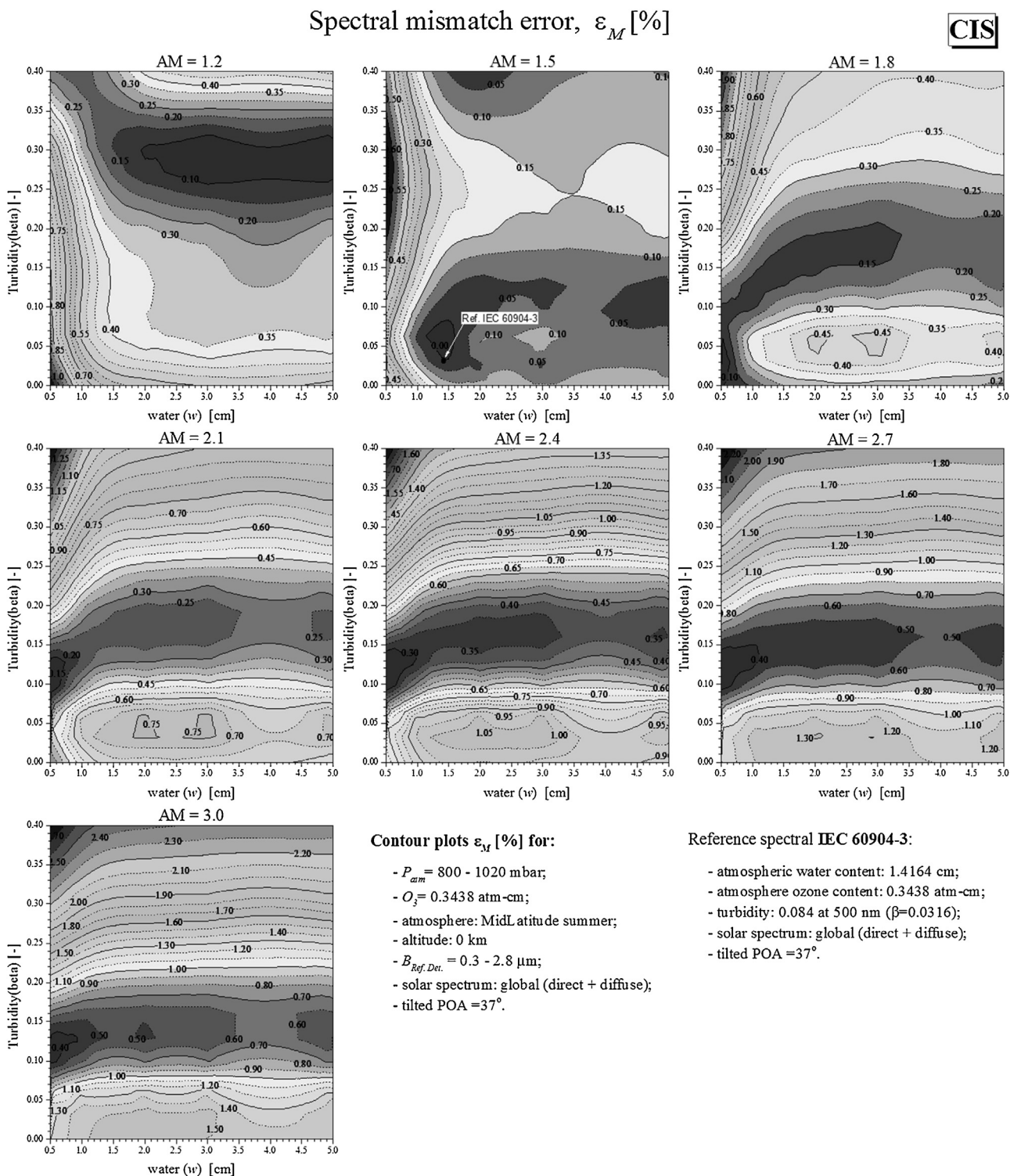


Fig. 21. Graphs of the spectral inconsistency error function (ε_M) for measurements of CIS cells/modules, in open space conditions on a cloudless day. The results refer to the summer period in Central Europe and the conditions presented in the background of the figure.

Spectral mismatch error, ε_M [%]

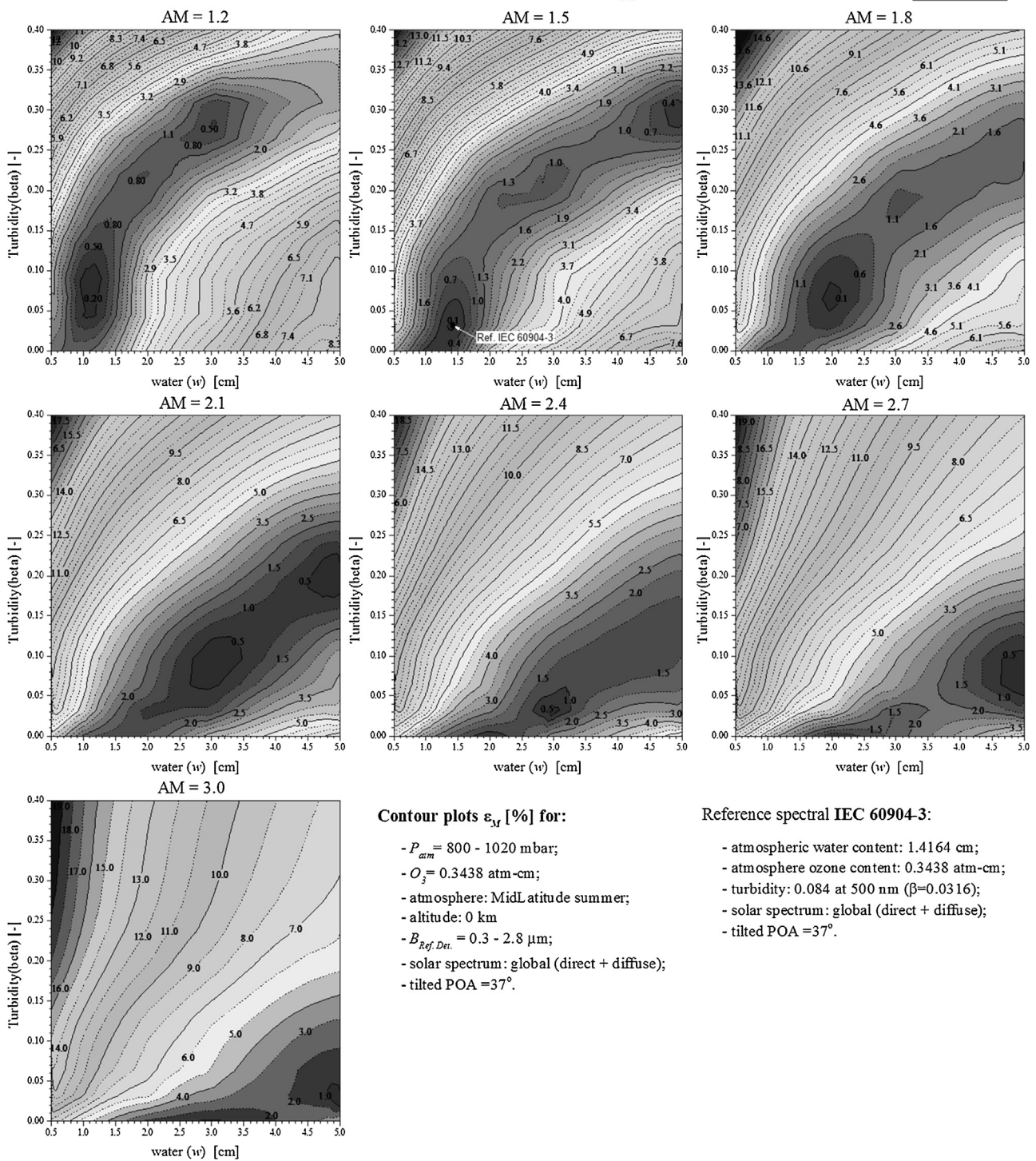
a_Si_SJ

Fig. 22. Graphs of the spectral inconsistency error function (ε_M) for measurements of a-Si_SJ cells/modules, in open space conditions on a cloudless day. The results refer to the summer period in Central Europe and the conditions presented in the background of the figure.

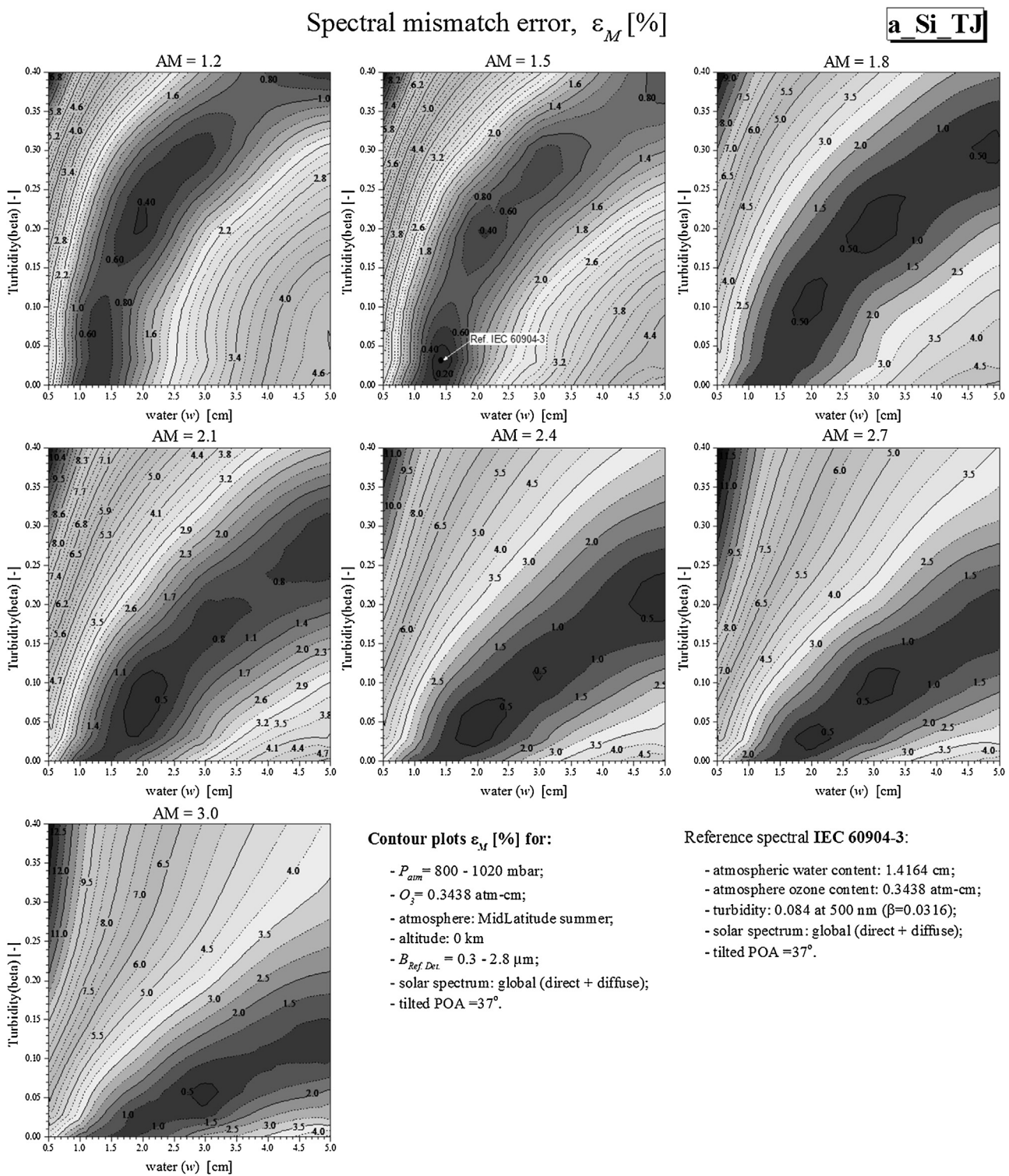


Fig. 23. Graphs of the spectral inconsistency error function (ε_M) for measurements of a-Si TJ cells/modules, in open space conditions on a cloudless day. The results refer to the summer period in Central Europe and the conditions presented in the background of the figure.

mass suppresses blue light and low content of steam does not absorb enough infra-red radiation). As pyranometer reacts much stronger to high-energy “blue photons” than a crystalline silicon cell, the cell current is amplified by the red spectrum area (the occurrence of the measuring points trajectory effect – see Fig. 13). Crystalline (c-Si), polycrystalline (mc-Si) and CIS modules, due to their very wide bandwidth of SR show little sensitivity to the changes of the solar spectrum distribution. The reaction is much

bigger in the modules from amorphous silicon, one- and three-junction, due to their much narrower spectral characteristics. They are very sensitive to the changes in the high-energy area of solar radiation spectrum.

- 4 The optimum conditions for testing cells and modules, which bring the smallest spectrum inconsistency errors, are:
 - 1) AM: optimum 1.2 (the lower the better). The lowest values occur in the summer.

Table 3

Atmospheric parameter values used in detailed simulation [37].

Air mass	1.2	1.5	1.8	2.1	2.4	2.7	3	0.4
Turbidity(β - beta)	0	0.02	0.05	0.1	0.2	0.3		
Precipitable water (w)	[cm]	0.5	1	2	3	5		
Atmosphere ozone content U_{O_3}		0.3438 atm-cm						
Reference atmosphere		MidLatitude summer						
Aerosol model		S&F Rural						
NO_2		use defaults from selected atmosphere (typical values for the above-mentioned area: 0.1 - exceptional bright sky, 1 - standard, 5 - clear smog in the atmosphere) [matm-cm]						
Surface pressure		1013.25 mb						
Latitude		52°						
Altitude		0 km						
Extraterrestrial spectrum		Gueymard 2002 (synthetic)						
Tilted POA		37°						
Spectral results		Global tilted irradiance B=(280 ; 2800) nm						

- 2) β : below 0.05. Higher values can be tolerated on condition that precipitable water content is also high.
 3) w (precipitable water): 1–3 cm – typical moderate climate conditions. Maximum 5 cm is allowed on condition that turbidity is not too low. Only subtropical and tropical locations will have such a high level of precipitable water, but turbidity will also be higher. The conditions below 1 cm should be avoided. If the air temperature is $<10^{\circ}\text{C}$, precipitable water will probably be below 1 cm. Therefore, studies carried out on high altitudes or during winter, may result in large inconsistency errors.

3.3. The principles of taking measurements of cells/modules with the use of natural sunlight

Measurements with natural sunlight depend on weather conditions. The first stage of the measuring procedure is to verify if the conditions are appropriate. The phrase “appropriate conditions” is relative, because this depends on the required precision of the measurement [38–40].

In order to determine if the conditions are appropriate, one should:

- Make sure that the sky is relatively cloud-free (the period when there are no clouds 30° from the Sun).
- Measure relative air humidity, air temperature, atmospheric pressure and solar radiation intensity.
- Calculate air mass according to (2), water content in the atmosphere (Fig. 15), turbidity (Fig. 14).
- From the spectral inconsistency error graph (ε_M), read for the selected cell/module, whether the measurement accuracy will be acceptable (Figs. 19–23).

Measurement [41,42]:

- Measure relative humidity, air pressure and temperature.
- Leave the pyrometer in order for the measurement to stabilise.
- Make sure that the radiation intensity is more stable in the range of 0.5% in time which is not shorter than the double time of pyranometer reaction.
- Check if there are no cloud formations near the Sun.
- Simultaneously measure radiation value, I-V characteristics and temperature of a cell/module.

Presentation:

- Draw a module current-voltage characteristics, pursuant to IEC 60904-1 [43] considering such conditions as radiation intensity and a cell temperature. The recommended temperature range for

cells and modules is between 25 and 50°C, and natural sunlight radiation intensity from 700 to 1 100 W/m².

- The adjustment of the obtained I-V characteristics for STC conditions, shall be carried out according to IEC 60 891 [44]. Individual measurement should be taken in similar conditions, i.e. the number of measurement adjustments should be minimised. Repeatability of individual measurements shall be higher than ± 1%.
- Define a cell/module basic technical parameters from I-V characteristics [45–48].

4. Conclusions

The following conclusions can be drawn from the carried out research:

- 1 All previously presented formulas for air mass determination, i.e., taken from Sandi - Eq. (2), SMART2 – (4) for Rayleigh's dispersion function, SEDES – (5) or SPECTRAL2 – (6), provide very similar results. Noticeable differences appear only for the angles much above 85° and do not exceed 0.5% for the angles up to 89°.
- 2 The main problem with measurements with sunlight is its large spectral changeability, which means that the measurement conditions with natural sunlight restrict its possibility. The measurements can be carried out only in the appropriate conditions. In natural conditions, even for the same day, spectral distribution of solar radiation of the same AM from before and after noon is different, which results in different measurement outputs for the same PV cells and modules (Fig. 13).
- 3 The optimum conditions for testing cells and modules, which bring the smallest spectrum inconsistency errors, are:
 - 1) AM: optimum 1.2 (the lower the better). The lowest values occur in summer.
 - 2) β : below 0.05. Higher values can be tolerated on condition that precipitable water content is also high.
 - 3) w (precipitable water): 1–3 cm – typical moderate climate conditions. Maximum 5 cm is allowed on condition that turbidity is not too low. Only subtropical and tropical locations will have such a high level of precipitable water, but turbidity will also be higher.
- 4 Crystalline (c-Si), polycrystalline (mc-Si) and CIS modules, due to their very wide bandwidth of SR show little sensitivity to the changes of the solar spectrum distribution. The reaction is much bigger in the modules from amorphous silicon, one- and three-junction, due to their much narrower spectral characteristics and they are very sensitive to changes in high-energy range of solar radiation spectrum.
- 5 The spectral inconsistency error is lower than the measurement error, occurring with any cheap simulator of sunlight, without

adjustment of spectral error. In practice, one can obtain the spectral error lower than 2% for the tested PV cells and modules, in optimum measurement taking conditions.

The authors allow to use the data from this article for the purpose of other research and publications, on condition of identifying the source of origin. The presented graphs in electronic form and other data may be offered individually, upon an e-mail request.

Acknowledgements

The authors wish to thank doctor engineer **Tadeusz Źdanowicz from Wrocław Technical University** and doctor engineer **Janusz Teneta from AGH Kraków** for disclosing their measurement data to carry out the above analyses, their help and assistance in implementing the study and editing this article.

References

- [1] F. Kasten, A. Young, Revised optical air mass and approximation formula, *Appl. Opt.* 28 (1989) 4735–4738, <http://dx.doi.org/10.1364/AO.28.004735>.
- [2] D.L. King, J.A. Kratochvil, W.E. Boyson, Measuring solar and angle-of-incidence effects on photovoltaic modules and solar irradiance sensor, in: 26th IEEE PVSC Anaheim, 1997 <http://www.pvsc-proceedings.org/>.
- [3] C. Gueymard, Parameterized transmittance model for direct beam and circumsolar spectral irradiance, *Sol. Energy* 71 (2001) 325–346, [http://dx.doi.org/10.1016/S0038-092X\(01\)00054-8](http://dx.doi.org/10.1016/S0038-092X(01)00054-8).
- [4] C. Gueymard, SMARTS2, a Simple Model of the Atmospheric Radiative Transfer of Sunshine. FSEC-PF-270-95, Florida Solar Energy Centre, Florida, 1995 <https://www.nrel.gov/grid/solar-resource/smarts.html>.
- [5] F.M. Miskolczi, High resolution atmospheric radiance-transmittance code (HARTCODE), in: Meteorology and Environmental Sciences, World Scientific, Singapore, 1990.
- [6] C. Whitaker, J. Newmiller, Photovoltaic Module Energy Rating Procedure. Final Subcontract Report. NREL Contract No. DE-AC36-83CH10093, Newmiller Endecon Engineering San Ramon, California, 1998 <https://www.nrel.gov/docs/legosti/old/23942.pdf>.
- [7] F. Kasten, Arch. Meteorol. Geophys. Bioclimat., 14 (1966) 206–211.
- [8] T. Rodziewicz, T. Źdanowicz, M. Żąbkowska-Wałkiewicz, Seasonal behaviour of different PV modules, *Chem. Inż. Ekol.* 9 (2002) 1241–1249.
- [9] M. Wałkiewicz, T. Rodziewicz, Ogniwa Słoneczne, Wpływ środowiska naturalnego na ich pracę [Solar cells. Impact of Natural Environment on Their Operation], PWN, Warszawa, 2010 (IN POLISH).
- [10] J.W. Spencer, Fourier series representation of the position of the sun, *Search* 2 (1971) 162–172.
- [11] D.J. Myers, Solar Applications in Industry and Commerce, Prentice-Hall, Inc., Englewood Cliffs, New Jersey, 1984 https://www.researchgate.net/publication/294774421_SOLAR_APPLICATIONS_IN_INDUSTRY_AND_COMMERCE.
- [12] H. Chenming, M.R. White, Solar Cells From Basics to Advanced System, McGraw-Hill Book Company, New York, 1983 <https://www.amazon.com/Solar-Cells-Advanced-ELECTRICAL-ENGINEERING/dp/0070307458>.
- [13] IEC 60904-3 ED4, Photovoltaic Devices – Part 3: Measurement Principles for Terrestrial Photovoltaic (PV) Solar Devices With Reference Spectral Irradiance Data, 2017 <http://www.iec.ch/dyn/www/f?p=103:23:0:::FSP.ORG.ID:1276>.
- [14] C.A. Gueymard, D. Myers, K. Emery, Proposed reference irradiance spectra for solar energy systems testing, *Sol. Energy* 73 (2002) 443–467 <https://www.sciencedirect.com/search?pub=Solar%20Energy&volume=73&page=443&show=25&sortBy=relevance&origin=jrnln.home&zone=search&cid=271459>.
- [15] C.A. Gueymard, Analysis of monthly average atmospheric precipitable water and turbidity in Canada and Northern United States, *Sol. Energy* 53 (1994) 57–71, [http://dx.doi.org/10.1016/S0038-092X\(94\)90606-8](http://dx.doi.org/10.1016/S0038-092X(94)90606-8).
- [16] C.A. Gueymard, Turbidity determination from broadband irradiance measurements: a detailed multcoefficient approach, *J. Appl. Meteorol.* 37 (1998) 414–435, [http://dx.doi.org/10.1175/1520-0450\(1998\)037<0414:TDFBIM>2.0.CO;2](http://dx.doi.org/10.1175/1520-0450(1998)037<0414:TDFBIM>2.0.CO;2).
- [17] T. Źdanowicz, Materials XII Optoelectronics School 22–24.05.1997, Kazimierz Dolny, Poland, 1997, 159.
- [18] D. Berman, D. Faiman, EVA browning and the time-dependence of I-V curve parameters on PV modules with and without mirror-enhancement in a desert environment, *Sol. Energy Mater. Sol. Cells* 45 (1997) 401–412 <https://www.sciencedirect.com/search?pub=Solar%20Energy%20Materials%20and%20Solar%20Cells&volume=45&page=401&show=25&sortBy=relevance&origin=jrnln.home&zone=search&cid=271495>.
- [19] T. Źdanowicz, T. Rodziewicz, M. Wałkiewicz, Effect of air mass factor on the performance of different type of PV modules, 3rd World Conference on Photovoltaic Energy Convers (2003) <http://www.pvsc-proceedings.org/>.
- [20] ANSI/ASTM E1362-99: Test Method for Calibration of Non-Concentrator Photovoltaic Secondary Reference Cells (revision of ANSI/ASTM E1362-95) - December 7, 1999 <https://infostore.saiglobal.com/en-gb/Standards/ASTM-E1362-99-983025/>.
- [21] ANSI/ASTM E1125-99: Standard Test Method for Calibration of Primary Non-Concentrator Terrestrial Photovoltaic Reference Cells Using a Tabular Spectrum. American Society for Testing and Materials, 100 Barr Harbor Drive, West Conshohocken, PA 19428-2959, USA, 1999, <https://infostore.saiglobal.com/en-gb/Standards/ASTM-E1125-99-982848/> <https://reference.globalspec.com/standard/3862597/astm-e1125-16>.
- [22] NASA TM 73702: Terrestrial Photovoltaic Measurement Procedures, TM 73 702, NASA, 1977 <https://www2.jpl.nasa.gov/adv.tech/photovol/2016CTR/LeRC%20-%20Terr%20PV%20Meas%20Proc.1977.pdf>.
- [23] R.L. Mueller, The calculated influence of atmospheric conditions on solar cell ISC under direct and global solar irradiances, Nineteenth IEEE Photovoltaic Specialists Conference, Proc (1987) 166–170 <http://www.pvsc-proceedings.org/>.
- [24] ASTM E1039-99: Standard Test Method for Calibration of Silicon Non-Concentrator Photovoltaic Primary Reference Cells Under Global Irradiation(revision of ANSI/ASTM E1039-94) (Withdrawn 2004), ASTM International, West Conshohocken, PA, 1999 <https://www.astm.org/Standards/E1039.htm>.
- [25] R.J. Matson, K.A. Emery, R.E. Bird, *Solar cells. Their science, Technol. Appl. Econ.* 11 (1984) 105–145.
- [26] W. Keogh, A.W. Blakers, Progress in photovoltaics, *Res. Appl.* 12 (2004) 1–19, <http://dx.doi.org/10.1002/pip.517>.
- [27] A. Angström, Techniques of determining the turbidity of the atmosphere, *Tellus* 13 (1961) 214–223, <http://dx.doi.org/10.1111/j.2153-3490.1961.tb00078.x>.
- [28] C. Gueymard, F. Vignola, Determination of atmospheric turbidity from the diffuse-beam broadband. Irradiance ratio, *Sol. Energy* 63 (1998) 135–146 <https://www.sciencedirect.com/search?pub=Solar%20Energy&cid=271459&volume=63&page=135&show=25&sortBy=relevance>.
- [29] F. Kasten, A simple parameterization of the pyrheliometric formula for determining the Linke turbidity factor, *Meteor. Rundschau* 33 (1980) 124–127 https://www.researchgate.net/publication/284652643_A.simple.parameterization.of.the.pyrheliometric.formula_for.determining.the.Linke.turbidity.factor.
- [30] F. Kasten, The Linke turbidity factor based on improved values of the integral Rayleigh optical thickness, *Sol. Energy* 56 (1996) 239–244 <https://www.sciencedirect.com/search?pub=Solar%20Energy&cid=271459&volume=56&page=239&show=25&sortBy=relevance>.
- [31] C.A. Gueymard, Assessment of the accuracy and computing speed of simplified saturation vapor equations using a new reference dataset, *J. Appl. Meteorol. Climatol.* 32 (1993) 1294–1300.
- [32] C. Gueymard, J.D. Garrison, Critical evaluation of precipitable water and atmospheric turbidity in Canada using measured hourly solar irradiance, *Sol. Energy* 62 (1998) 291–307 <https://www.sciencedirect.com/search?pub=Solar%20Energy&cid=271459&volume=62&page=291&show=25&sortBy=relevance>.
- [33] M. Krawczynski, M.B. Strobel, C.J. Hibberd, T.R. Betts, R. Gottschalg, Proc. 25th EU PVSEC, 2010, pp. 4710–4714 <https://www.eupvsec-proceedings.com/>.
- [34] T. Minemoto, M. Toda, S. Nagae, M. Gotoh, A. Nakajima, K. Yamamoto, H. Takakura, Y. Hamakawa, Effect of spectral irradiance distribution on the outdoor performance of amorphous Si/thin-film crystalline Si stacked photovoltaic modules, *Sol. Energy Mater. Sol. Cells* 91 (2007) 120–122, <http://dx.doi.org/10.1016/j.solmat.2006.07.014>.
- [35] Kipp & Zonen: <http://www.kippzonen.com/>.
- [36] Kipp, Zonen, Instruction Manual CM 21. Precision Pyranometr, 2019, pp. 17 <http://www.kippzonen.com/>.
- [37] C. Gueymard, SMARTS Code, Version 2.9.2, USER'S MANUAL, Solar Consulting Services, 2005 https://reddc.nrel.gov/solar/models/smarts/SMARTS295.users.manual_pc.pdf.
- [38] G. TamizhMani, K. Paghsian, J. Kuitche, M. Gupta, G. Sivasubramanian, Photovoltaic module power rating per IEC 61853-1 standard – a study under natural sunlight, Solar ABCs Study Report (2011), March 2011 www.solarABCs.org <http://www.iec.ch/dyn/www/f?p=103:23:0:::FSP.ORG.ID:1276>.
- [39] IEC 61 724.: Photovoltaic System Performance Monitoring - Guidelines for Measurement, Data Exchange and Analysis, EC, Geneva, 1998 <http://www.iec.ch/dyn/www/f?p=103:23:0:::FSP.ORG.ID:1276>.
- [40] C.N. Long, T.P. Ackerman, K.L. Gaustad, J.N.S. Cole, Estimation of fractional sky cover from broadband shortwave radiometer measurements, *J. Geophys. Res.* 111 (2006), D11204, <http://dx.doi.org/10.1029/2005JD006475>.
- [41] IEC 60904-2, 2nd Edition, 2006.: International Electrotechnical Commission, Requirements for Reference Solar Devices, Geneva, 2006 <http://www.iec.ch/dyn/www/f?p=103:23:0:::FSP.ORG.ID:1276>.
- [42] IEC 60 904-6, 2nd Edition, 2006.: Requirements for Reference Solar Modules, Geneva, 2006 <http://www.iec.ch/dyn/www/f?p=103:23:0:::FSP.ORG.ID:1276>.
- [43] IEC 60 904-1.: Photovoltaic Devices - Part 1: Measurement of Photovoltaic Current-voltage Characteristics, IEC, Geneva, 1987 <http://www.iec.ch/dyn/www/f?p=103:23:0:::FSP.ORG.ID:1276>.
- [44] IEC 60 891, 3rd Edition, 2017.: Photovoltaic Devices - Procedures for Temperature and Irradiance Corrections to Measured I-V Characteristics,

- Geneva, 2017 http://www.iec.ch/dyn/www/f?p=103:23:0::::FSP_ORG_ID:1276.
- [45] IEC 60 904-10, 2nd Edition, 2006.: Methods of Linearity Measurement, Geneva, 2006 http://www.iec.ch/dyn/www/f?p=103:23:0::::FSP_ORG_ID:1276.
- [46] S. Corrs, M. Böhm, Validation and comparison of curve correction procedures for silicon solar cells, Proc 13th PVSEC (1995) <https://www.eupvsec-proceedings.com/>.
- [47] Y. Tsuno, Y. Hishikawa, K. Kurokawa, Temperature and Irradiance Dependence of the I-V Curves of Various Kinds of Solar Cells, Technical Digest of the PVSEC 15, Shanghai, 2005, 422.
- [48] IEC 60 904-5, 2nd Edition 2006.. Determination of Equivalent Cell Temperature (ECT)of Photovoltaic (PV) Devices by the Open-circuit Voltage Method, Geneva, 2006 http://www.iec.ch/dyn/www/f?p=103:23:0::::FSP_ORG_ID:1276.